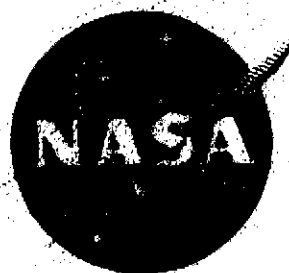


NASA CR-134609

BCAC D6-41521



727 AIRPLANE SIDE INLET LOW-SPEED PERFORMANCE

CONFIRMATION MODEL TEST FOR REFANNED

JT8D ENGINES

(NASA-CR-134609) THE 727 AIRPLANE SIDE
INLET LOW-SPEED PERFORMANCE CONFIRMATION
MODEL TEST FOR REFANNED JT8D ENGINES
(Boeing Commercial Airplane Co., Seattle)
82 p HC \$7.25

N74-20661

Unclas
35579

G3/02

CSCL 01C

by A. L. Schuehle

BOEING COMMERCIAL AIRPLANE COMPANY

A DIVISION OF
THE BOEING COMPANY

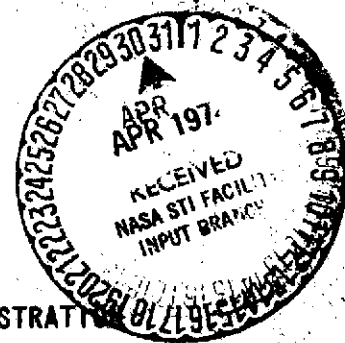
PRICES SUBJECT TO CHANGE

Prepared for

NATIONAL AERONAUTICS AND SPACE ADMINISTRATION

NASA Lewis Research Center

Contract NAS3-17842



Reproduced by
NATIONAL TECHNICAL
INFORMATION SERVICE
US Department of Commerce
Springfield, VA. 22151

N O T I C E

THIS DOCUMENT HAS BEEN REPRODUCED FROM THE
BEST COPY FURNISHED US BY THE SPONSORING
AGENCY. ALTHOUGH IT IS RECOGNIZED THAT CER-
TAIN PORTIONS ARE ILLEGIBLE, IT IS BEING RE-
LEASED IN THE INTEREST OF MAKING AVAILABLE
AS MUCH INFORMATION AS POSSIBLE.

1. Report No. CR-134609	2. Government Accession No.	3. Recipient's Catalog No.	
4. Title and Subtitle 727 Airplane Side Inlet Low-Speed Performance Confirmation Model Test for Refanned JT8D Engines		5. Report Date March 1974	
		6. Performing Organization Code	
7. Author(s) A. L. Schuehle		8. Performing Organization Report No. D6-41521	
		10. Work Unit No.	
9. Performing Organization Name and Address Boeing Commercial Airplane Company P.O. Box 3707 Seattle, Washington 98124		11. Contract or Grant No. NAS3-17842	
		13. Type of Report and Period Covered Contractor Report	
12. Sponsoring Agency Name and Address National Aeronautics and Space Administration Washington, D.C. 20546		14. Sponsoring Agency Code	
15. Supplementary Notes Project Manager, A. A. Medeiros NASA Lewis Research Center, Cleveland, Ohio 44135			
16. Abstract This report presents the results of a low-speed wind tunnel test of a 0.3 scale model 727 airplane side inlet for Pratt & Whitney Aircraft JT8D-100 engines. The test was conducted by the Propulsion Technology Staff of the Boeing Commercial Airplane Company under authorization of NASA Contract NAS3-17842, "Phase II Program on Ground Test of Refanned JT8D Engines and Nacelles for the 727 Airplane". The objectives of the test were to develop lines for a full-scale flightworthy inlet, to evaluate inlet total pressure recovery and steady-state total pressure distortion, and to obtain model-scale distortion data which can be used in the assessment of the compatibility of the inlet with the JT8D-100 series engines. A secondary objective was to obtain internal/external cowl static pressures for the determination of nacelle loads. Two basic inlet models were tested at static, forward speed, angle-of-attack (inflow angle), and cross-wind conditions. One model was with and one without an acoustic ring. Two modifications to the models were also tested, one with the ring closer to the inlet throat and one with a larger lip. Test measurements consisted of inlet surface static pressure, engine face total pressure, inlet airflow, tunnel total pressure, tunnel total temperature and tunnel velocity. Total pressure traverses were taken directly behind the ring and strut. No dynamic measurements were taken. Test results indicate acceptable inlet total pressure recovery and total pressure distortion at static, forward speed, and angle-of-attack conditions. At cross-wind conditions, the two basic inlets had acceptable distortion at 11 knots cross wind, but the distortion became marginal when compared to the Pratt & Whitney Aircraft limits at 20 knots cross wind.			
17. Key Words (Suggested by Author(s)) 727 Airplane Side Inlet Inlet Pressure Recovery and Distortion Refanned JT8D Engine Inlet Wind Tunnel Test		18. Distribution Statement Unclassified - Unlimited	
19. Security Classif. (of this report) Unclassified	20. Security Classif. (of this page) Unclassified	21. No. of Pages 80	22. Price*

* For sale by the National Technical Information Service, Springfield, Virginia 22151

FOREWORD

The low-speed wind tunnel test described in this report was performed by the Propulsion Technology Staff of the Boeing Commercial Airplane Company, A Division of The Boeing Company, Seattle, Washington. The work, sponsored by NASA Lewis Research Center and reported herein, was performed between October 1973 and February 1974.

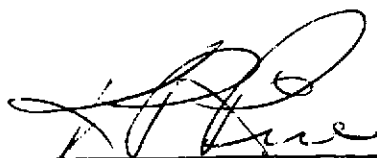
This report has been reviewed and is approved by:


L. J. Winslow, Group Engineer
Propulsion Technology Staff

22 MARCH 1974
Date


J. A. Ferrell
Chief, Staff Technology
JT8D Refan Program

22 MARCH 1974
Date


K. P. Rice
Program Manager
JT8D Refan Program

3/28/74
Date

Preceding page blank

TABLE OF CONTENTS

	<u>Page</u>
1.0 SUMMARY -----	1
2.0 INTRODUCTION -----	5
2.1 BACKGROUND -----	5
2.2 INLET DESIGN -----	6
2.2.1 Design Constraints and Goals -----	6
2.2.2 Design Procedure -----	7
3.0 MODEL AND TEST DESCRIPTION -----	11
3.1 MODEL DESCRIPTION AND MODEL INSTRUMENTATION-----	11
3.2 TEST FACILITY AND FACILITY INSTRUMENTATION-----	12
3.3 TEST PROCEDURE AND TEST CONDITIONS -----	13
3.4 DATA REDUCTION AND PRESENTATION -----	15
4.0 RESULTS AND DISCUSSION -----	17
4.1 SURFACE MACH NUMBER DISTRIBUTION -----	17
4.2 TOTAL PRESSURE RECOVERY -----	17
4.3 TOTAL PRESSURE DISTORTION -----	19
4.3.1 Engine Face Pressure Recovery Maps -----	19
4.3.2 Pratt & Whitney Aircraft Distortion-----	20
Criteria	
4.4 COMPARISON WITH EXISTING 727 SIDE INLET -----	23
4.4.1 Inlet Geometry and Airflow -----	23
4.4.2 Total Pressure Recovery -----	24
4.4.3 Total Pressure Distortion -----	24
5.0 CONCLUSIONS -----	25
6.0 FIGURES-----	27
APPENDIX A - SYMBOLS -----	71
APPENDIX B - INLET COORDINATES -----	75
REFERENCES -----	79

1.0 SUMMARY

A low-speed performance confirmation model test was conducted for a Boeing 727 airplane side engine inlet designed for use with refanned JT8D engines (designated the JT8D-100 series). The test was conducted in the Boeing Low-Speed Wind Tunnel located at North Boeing Field, Seattle, Washington.

The objectives of the test were:

- To develop lines for a full-scale flightworthy inlet, for ground test, with performance (total pressure recovery and distortion) comparable to the existing 727 side inlet.
- To evaluate inlet total pressure recovery and steady-state total pressure distortion of the side engine inlet at JT8D-100 engine airflows at low-speed and cross-wind conditions.
- To obtain model-scale distortion data which can be used in the assessment of the compatibility of the inlet with the JT8D-100 series engines.

A secondary objective of the test was to obtain internal/external cowl static pressures for the determination of nacelle loads.

Two basic 0.3 scale models ($A_{HI}/A_{TH} = 1.25$), without acoustic treatment, were tested at static, forward speed, angle-of-attack (inflow angle), and cross-wind conditions. The two models were without an acoustic ring (Configuration 1) and with an acoustic ring (Configuration 2). Two inlets were designed and tested so that full-scale ground test hardware fabrication could proceed on the basis that either inlet Configuration 1 or 2 could be ground tested. Two modifications to these basic models were tested at a selected number of conditions. The modifications consisted of using a larger lip (Configuration 1L,

$A_{HI}/A_{TH} = 1.30$) to investigate improved cross-wind performance; and moving the acoustic ring leading edge closer to the throat (Configuration 2R) to obtain more acoustic surface area.

Test measurements consisted of inlet internal and external surface static pressure, engine face total pressure, inlet airflow, tunnel total pressure, tunnel total temperature, and tunnel velocity. Total pressure traverses were taken directly behind the ring and strut. No dynamic measurements were taken.

Conclusions drawn from the test are:

- The cruise and angle-of-attack recovery and distortion of the Configuration 1 inlet, accounting for acoustic treatment, will be slightly better than that of the existing 727 inlet.
- The cruise recovery of the Configuration 2 inlet, excluding acoustic treatment, will be slightly lower (0.003) than that of the Configuration 1 inlet.
- The Configuration 1 and 2 inlets have an acceptable distortion at 11 knots cross wind, but the distortion becomes marginal when compared to the Pratt & Whitney Aircraft limit at 20 knots cross wind. The 30 knot cross-wind condition at 70 knots forward speed (cross wind/rolling takeoff) shows an acceptable distortion level. The two inlets were designed using a throat Mach number and lip contour that give an equivalent or slightly better cross-wind performance than the existing 727, and using normal operating procedures cross-wind performance should not present a problem. For a small cruise performance penalty, Configuration 1L will provide additional static cross-wind capability (up to 30 knots).

- The acoustic ring of Configuration 2 provides a baffling effect, when compared to Configuration 1, keeping the low pressure distorted flow in the outer annulus. This results in a "clean" core flow at all test conditions.
- The Configuration 2R inlet showed that the ring leading edge may be moved further into the throat, thus providing more acoustic treatment area, without a static, cross-wind or angle-of-attack recovery or distortion penalty.

2.0 INTRODUCTION

2.1 BACKGROUND

The Pratt & Whitney Aircraft JT8D-100 engine is a derivative of the basic JT8D turbofan engine modified to incorporate a new larger diameter, single-stage fan with a bypass ratio of 2.0 and two supercharging low-pressure compressor stages. The modification lowers jet noise, increases takeoff and cruise thrust, and lowers specific fuel consumption. The use of a JT8D-100 series engine, also referred to as a refanned JT8D, on the Boeing 727 airplane requires a larger side engine inlet due to the increased engine diameter and increased engine airflow. A new airplane nacelle for JT8D-100 series engines is currently being developed through a joint Boeing/NASA effort.

Two side inlet configurations have been designed for the nacelle. The inlets were designed considering inlet acoustic performance. The design and test results of the two inlets, along with test results for two modifications to these inlets, are the subjects of this report. The test evaluated the inlet internal aerodynamic performance at low-speed and cross-wind conditions using 0.3 scale models. The test was conducted during November and December 1973, in the Boeing Low-Speed Wind Tunnel, located at North Boeing Field, Seattle, Washington.

The objectives of the test were:

- To develop lines for a full-scale flightworthy inlet, for ground test, with a performance (total pressure recovery and distortion) comparable to the existing 727 side inlet.
- To evaluate the inlet total pressure recovery and steady-state total pressure distortion of the side engine inlet at JT8D-100 engine airflows at low-speed and cross-wind conditions.

Preceding page blank

- To obtain model-scale distortion data which can be used in the the assessment of the compatibility of the inlet with the JT8D-100 series engines.

A secondary objective of the test was to obtain internal/external cowl static pressures for the determination of nacelle loads.

This test was performed under authorization of NASA Contract NAS33-17842, "Phase II Program on Ground Test of Refanned JT8D Engines and Nacelles for the 727 Airplane," to support the development of a new 727 side engine inlet.

2.2 INLET DESIGN

2.2.1 Design Constraints and Goals

The following constraints were imposed on the side inlet design:

- The inlet diameter at the engine face (D_2) shall be 50.1 inches.
- To avoid interference with galley door access the inlet length to diameter ratio (L/D_2) shall not be greater than 0.8.
- Two inlets shall be designed, one with and one without an acoustic splitter ring.
- The inlet corrected airflow capability shall be as follows:
 - (1) 467 lb/sec at takeoff, sea level static condition, std. day.
 - (2) 480 lb/sec at MCR, $0.8M_\infty$, 30,000 ft., std. day.
 - (3) 501 lb/sec at MCT, $0.6M_\infty$, 35,000 ft., std. day.

The maximum JT8D-100 engine cold day airflow at both sea level and 10,000 ft., -60°F ambient temperature, is 516 lb/sec. Applying a +3 percent production engine airflow tolerance results in a 531.5 lb/sec maximum airflow.

- The inlet angle-of-attack (inflow angle) capability shall be greater than or equal to the angles measured during the Reference 1 wind tunnel flowfield test. The maximum angle measured during the test was found to be a 17 degree downwash angle relative to the engine centerline during unstalled wing operation.

The following design goals were set:

- A cross-wind capability equivalent to or better than the existing 727 production side inlet.
- Total pressure distortion and recovery levels, for the inlet without an acoustic ring, equivalent to or better than the existing 727 production inlet.

2.2.2 Design Procedure

A number of inlets, both with and without acoustic splitter rings, have been designed and model tested during past studies at the Boeing Company. The design procedure evolved from these past studies was generally followed in this design. This involves laying out a lip, diffuser, and centerbody contour which accounts for the following:

- internal flow considerations
- acoustic considerations
- engine airflow schedule
- inlet angle-of-attack (inflow angle)
- inlet cross-wind capability
- external aerodynamic considerations
- manufacturing considerations

The empty inlet potential flow field is then computed using an axially symmetric, compressible, potential flow computer analysis. The contours are then modified if the potential flow results indicate flow regions which may be improved. If the inlet is to be used with an acoustic ring the empty inlet contours are

designed so as to accommodate the added blockage due to the ring. The ring contour is then wrapped around the potential flow streamline (particular streamline dictated by acoustic considerations) with a new potential flow field being computed after the ring insertion. The placing of the splitter around the natural streamline should produce the least amount of flow disturbance. Further refinements in the contours are then made if flow field results indicate improvements can be made. No account is made in the potential flow computations for the struts which support the ring.

Based on the Reference 2 high speed nacelle drag test it was determined that axially symmetric side inlets with a highlight diameter of 52.2 inches would be satisfactory. A lip contraction ratio (A_{HI}/A_{TH}) of 1.25, identical to the present 727, was selected since the present 727 lip has not presented problems during operation. Based on other Boeing studies a super ellipse $[(\frac{x}{a})^{2.2} + (\frac{y}{b})^{2.2} = 1]$ was selected for the lip contour. The highlight diameter and specified contraction ratio yield a throat area (1712.81 inches²) which gives a one dimensional cruise throat Mach number similar to the existing 727 with JT8D-1 or -7 engines. At a corrected airflow of 480 lb/sec. the JT8D-100 inlet throat Mach number is 0.57. Based on manufacturing considerations it was decided to make all internal surfaces axially symmetric. This could be done and still meet the angle-of-attack and cross-wind objectives discussed in Section 2.2.1.

The design procedure was applied to develop inlets with and without an acoustic ring. Early in the design it was decided that a common lip, diffuser, and nose dome would be used for the two inlets. This common aspect makes it possible to decide later in the development phase whether or not to use an acoustic ring. It also makes it impossible to truly optimize both

configurations, though with the relatively thin acoustic ring (0.7 inches full scale) the penalty is small.

The two inlet configurations are shown in Figure 1. Configuration 1 is without and Configuration 2 with the acoustic ring. Figures 2 and 3 show the Mach number distributions obtained from the potential flow analysis. All analyses were done using the 480 lb/sec cruise corrected airflow. The Configuration 2 ring leading edge location was selected based on the intersection of the near static ($V_{\infty} = 15$ knots) and forward speed ($M_{\infty} = .8$) streamlines as shown on Figure 2, and, on past Boeing work. The ring trailing edge is one inch upstream of the engine face. This provides ring removal clearance with a near maximum of acoustic surface for the inlet length constraint. This also allows a substantial distance (approximately 14 inches) between the ring trailing edge and the first stage fan. The ring radial location, determined from acoustic considerations, is on the streamline which is equidistant from the cowl and nose dome at the engine face.

For reference purposes the one dimensional throat and engine face Mach numbers as a function of corrected airflow and the one dimensional area distribution for the two inlets are shown in Figure 4. It should also be pointed out that on the refan engine the nacelle slopes 3 degrees out from the airplane body buttock line and 3 degrees 22 minutes up from the airplane body water line. This is approximately the same on the existing 727 nacelle.

3.0 MODEL TEST DESCRIPTION

3.1 MODEL DESCRIPTION AND MODEL INSTRUMENTATION

The inlets tested were 0.2994 scale axially symmetric aluminum models. All wall surfaces were hardwall, therefore without acoustic material. In addition to the Configuration 1 and 2 inlets described in the previous section two modifications to these basic inlets were also tested. An additional lip ($A_{HI}/A_{TH} = 1.30$, Configuration 1L) was tested at cross-wind conditions to determine the potential for improved cross-wind performance. A ring and centerbody assembly (Configuration 2R), built for the NASA Phase I Refan Program, was tested to evaluate extending the ring leading edge closer to the inlet throat. All four inlet configurations, shown in Figure 5, used a common diffuser. Configurations 1 and 2 internal contours are identical to that currently being developed for the full-scale ground test. The strut contour and strut circumferential spacing have been changed slightly on the full-scale Configuration 2 inlet. A tabulation of the coordinates for all four models is given in Appendix B.

The models were tested without fuselage simulation at static, forward speed, and angle-of-attack conditions. The airplane fuselage was simulated during static and cross-wind testing, the windward side inlet being tested. Photos of the model in the cross-wind and forward speed installation and a view into the inlet are shown in Figures 6, 7, and 8 respectively. Figure 9 shows a sketch of the inlet in the cross-wind and forward speed installations.

A total of 57 static ports were utilized on the Configuration 1 inlet, 77 on Configuration 2. Configuration 1L and 2R utilized the eight engine face static pressure ports only. Figure 10 shows the location of the static ports.

Engine face total-pressure measurements were made using an existing fifteen-inch diameter, four-arm (16 probes per arm) rotating rake. The closest total pressure probes to the cowl and nose dome being 0.15 inches model scale. Measurements were taken at angular increments of 15 degrees. For a portion of the test conditions two total pressure traversing probes, located 180 degrees apart at the engine face, were used to obtain a detailed definition of the strut and ring wakes. Figure 11 shows a sketch of the rotating rake and traversing probes. Only steady state measurements were taken during the test.

3.2 TEST FACILITY AND FACILITY INSTRUMENTATION

The test was conducted in the Boeing Low-Speed Wind Tunnel "B" facility. The tunnel contains a 9 foot by 9 foot square test section. An Allison 501-D13 gas turbine driving a variable pitch propeller is used to draw atmospheric air through the bellmouth, flow straighteners, and test section. The test section airspeed could be varied from approximately 0 to 180 knots. Engine airflow simulation was obtained by using a General Electric J-47 turbojet engine as a pumping source. Air was drawn through the inlet model, a venturi meter and into the engine. Venturi airflow measurements were accurate to within ± 1 percent of the measured value. A 19 percent blockage screen (0.41 inch mesh with 0.041 inch diameter wire) was used for most test conditions. The screen was located as near the fan face station as possible (4-3/4 inches model scale from the engine face) in order to simulate the upstream effects of the fan rotor on the flow. With the screen installed the inlet choked at a simulated full scale corrected air flow of 502 lb/sec. Without the screen airflows in excess of 570 lb/sec. were possible.

Tunnel total and static pressure, tunnel total temperature and venturi temperatures and pressures were recorded for each test

condition. This steady-state data along with the model steady state data were recorded on the standard 9 x 9 Low Speed Wind Tunnel data acquisition system. This system, a Hewlett-Packard Dymec 2010D, is a trap and scan scannivalve system with output on punched paper tape. The capability of monitoring on-line engine RPM and a selected number of static pressures was available for setting test conditions.

3.3 TEST PROCEDURE AND TEST CONDITIONS

After the model was assembled, leak checked, and the instrumentation zero checked, the tunnel velocity and inlet airflows were set and allowed to stabilize for at least 30 seconds. Data were then recorded at various rake angles (at 15 degree increments between 7.5 and 82.5 degrees). Model surface pressure measurements were recorded at the first rake angle only.

Data were taken for static, crosswind and angle-of-attack (0 to 22.5 degrees) conditions. Data were taken for a full scale corrected airflow range of 180 to approximately 502 lb/sec with the screens and up to 560 lb/sec without the screens. Table 1 shows a summary of the test conditions at which the various models were tested. As shown on Table I the inlet angle of attack is actually a downwash due to the presence of the wing. Because of facility limitations all angles were in the upwash direction for the test model. Thus to go from the model test configuration to the airplane configuration all angles-of-attack results must be rotated by 180 degrees. The 76 knot, 22.5 degree installation simulates a 30 knot cross-wind 70 knot forward speed condition. The higher velocities at 22.5 degrees were run for the determination of nacelle loads. The nacelle loads results are reported in Reference 3.

TABLE I

CONFIGURATION NO. 1

INLET ANGLE-OF-ATTACK

RUN NUMBER $\alpha=0^\circ, 17.5^\circ, 22.5^\circ, 0^\circ$
 $\beta=0^\circ, 0^\circ, 0^\circ, 90^\circ$ ①

Tunnel Velocity, V_T ~ Knots

0	41			1
	42			
11				4
20				3
30				2
35	45			
70	44			
76			47	
180	43	46		

CONFIGURATION NO. 2

INLET ANGLE-OF-ATTACK

RUN NUMBER $\alpha=0^\circ, 14.8^\circ, 17.5^\circ, 22.5^\circ, 0^\circ$
 $\beta=0^\circ, 0^\circ, 0^\circ, 0^\circ, 90^\circ$ ①

Tunnel Velocity, V_T ~ Knots

0	39				12
					13
					17 ②
10					14
20					15
					18 ②
					20 ③
30					16
					19 ②
					21 ③
35	38				
70	37				
76				26	
100		48 ④	28 ④ 31 33	22 ④ 27	
120				23 ④	
150		49 ④	29 ④ 32 34	24 ④	
180	36 40 ②	50 ④ 51	30 ④ 35	25 ④	

CONFIGURATION NO. 1L

INLET ANGLE-OF-ATTACK

RUN NUMBER $\alpha=0^\circ$
 $\beta=90^\circ$ ①

Tunnel Velocity, V_T ~ Knots

0	5 ⑤
10	6 ⑤
20	7 ⑤
30	8 ⑤

CONFIGURATION NO. 2R

INLET ANGLE-OF-ATTACK

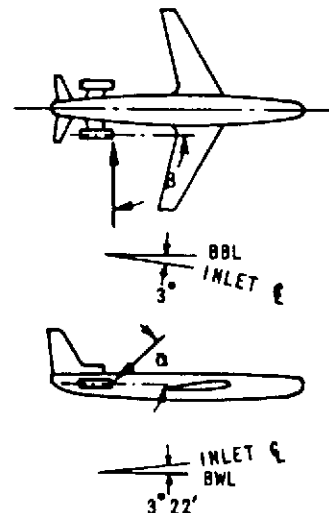
RUN NUMBER $\alpha=17.5^\circ, 0^\circ$
 $\beta=0^\circ, 90^\circ$ ①

Tunnel Velocity, V_T ~ Knots

0	9
20	10
30	11
180	52

NOTES:

- ① Cross wind ($\beta=90^\circ$) with fuselage except as noted, other conditions without fuselage.
- ② Without screens also.
- ③ Without fuselage.
- ④ Static pressure data only.
- ⑤ Without screens only.



3.4 DATA REDUCTION AND PRESENTATION

During the test program data were reduced using a standard Boeing data reduction computer program for inlet tests. Data were reduced using a quick look and final reduction version of the program.

Quick-look data were obtained by processing the punched paper tape through the Boeing Mechanical Laboratories SDS 92 computer. The tabular output consisted of total and static pressure measurements, surface Mach number distributions, surface pressure coefficients, surface pressure ratios, the rotating rake pressure array, inlet recovery, inlet airflow, and the steady-state distortion parameter $(P_{T \text{ Max}} - P_{T \text{ Min}})/P_{T2}$.

Additional quick look (on line) data were obtained from the test facilities own PDP8 computer. This consisted of tunnel conditions, inlet airflow, and the rotating rake pressure array.

Final data were obtained by generating a magnetic tape from the paper tape and processing it through the Boeing CDC 6600 computer. The final data consisted of tabular information similar to that obtained from the quick look data plus the distortion parameters defined by Pratt & Whitney Aircraft (see Section 4.3.2). Engine face plots showing lines of constant total pressure recovery were also generated on the CDC 6600 computer. All final data are permanently stored on microfilm.

The total pressure recovery measurements $(P_{T2}/P_{T\infty})$ presented in this document are computed on an area-average basis. The cowl wall region is handled by taking the average of the wall static pressure measurement and the closest total pressure probe multiplied by the annular area segment between the two. Inter-

mediate regions are handled by multiplying the annular area segment between any two probes by the average of their total pressures. The nose dome wall region is computed by taking a straight line fit from the last two total pressure probes to the wall. The nose dome was handled in this manner because its boundary layer is very thin, and of a high power law exponent, and straight line fitting to the wall static pressure would over estimate the loss in this region.

All airflow data presented in this report have been converted from 0.2994 model scale to full scale values.

4.0 RESULTS AND DISCUSSION

4.1 SURFACE MACH NUMBER DISTRIBUTION

Surface Mach number distributions at zero and 17.5 degrees angle of attack are shown in Figures 12 and 13 for Configurations 1 and 2 respectively. The analytical results plotted in the figures, are in good agreement with the data for the region from near the throat to the engine face. In the lip region the results differ since the analysis was done for a $M_{\infty} = .8$ whereas the data is for a $V_T = 180$ knots. At 17.5 degrees inlet angle of attack lip Mach numbers in excess of 1.3 were measured on the lower lip, the internal surface Mach numbers downstream of the throat remaining approximately the same.

4.2 TOTAL PRESSURE RECOVERY

Configuration 1 total pressure recoveries at static, cross-wind, forward speed, and angle-of-attack conditions are shown in Figures 14 and 15. As shown in Figure 14 at cross-wind velocities greater than 11 knots the recovery deteriorates rapidly. Figure 15 shows the recovery at the static condition with and without the fuselage. Without the fuselage a vortex was visually observed at static conditions coming off the tunnel side wall. This was also observed in the engine face measurements and accounts for the lower recovery without the fuselage at higher inlet airflows. At the angle-of-attack conditions, of 22.5 and 17.5 degrees the inlet shows high recoveries. At the 70 knot forward speed condition, shown on Figure 15, the inlet recovery level is nearly as high as that measured at 180 knots.

Configuration 2 total pressure recoveries at static, cross-wind, forward speed, and angle-of-attack conditions are shown in Figures 16 and 17. The same type of statements can be made

concerning the Configuration 2 inlet performance as were made for the Configuration 1 inlet, except, that due to the ring surface area the recovery level is lower. There was no evidence of ring leading edge separation at the static, forward speed or angle-of-attack conditions. The inlet was tested without the screens and without the fuselage at static and cross-wind conditions. For the static condition the presence of the screens made little difference in the recovery; but, at the cross-wind condition of 30 knots the screens provided an improvement in the recovery as shown in Figure 16. The presence of the fuselage provided some improvement at the static condition as shown in Figure 17 and a substantial improvement at the 20 and 30 knot cross-wind conditions as shown in Figure 16. The inlet recovery did not vary substantially over the range of tunnel velocities and angle-of-attack conditions tested as shown in Figure 17. As with the Configuration 1 inlet the Configuration 2 pressure recovery at 70 knots forward speed is nearly as high as that at 180 knots.

Total pressure traverses of the ring wake and strut wakes were taken at the engine face for the Configuration 2 inlet. Figure 18 shows a portion of the results. At the cruise airflow a minimum pressure ratio ($P_T/P_{T\infty}$) of 0.88 was measured behind the ring and 0.958 behind the struts. By integrating the ring and wake traverse measurements of Figure 18 (assuming the wake does not change along the trailing edge) the loss due to the strut and ring may be estimated. The cowl and nose dome loss may be obtained from rotating rake measurements, along with a second measurement of the ring loss. When this is done the total pressure loss (1-recovery, where the recovery is as discussed in Section 3.4) for each component of the Configuration 1 and 2 inlets at a corrected airflow of 481 lb/sec is as follows:

	Loss (1-Recovery)	
Cowl	0.0050	} Configuration 1 and 2
Nose Dome	0.0000	
Ring	0.0030	} Configuration 2
Struts	<u>0.0003</u>	
Total	0.0083	

The static and cross-wind recovery measurements of the Configuration 1L inlet are shown in Figure 19. Because of the high contraction ratio ($A_{HI}/A_{TH} = 1.30$) the inlet showed high recovery levels even at the 30 knot cross-wind condition.

The static, angle-of-attack and cross-wind recovery of the Configuration 2R inlet is shown in Figure 20. The recovery levels measured on the 2R model are comparable to the Configuration 2 model indicating that the Configuration 2 acoustic ring leading edge may be extended closer to the throat.

4.3 TOTAL PRESSURE DISTORTION

4.3.1 Engine Face Pressure Recovery Maps

Engine face pressure recovery maps show lines of constant steady state total pressure recovery at the engine face station. Such maps are useful as a visual aid. Although recovery maps were made for all test conditions only a select few are shown. These consist of:

- Figure 21 Configuration 1 at 180 knots and $\alpha = 17.5^\circ$
- Figure 22 Configuration 1 at 20 knots cross wind
- Figure 23 Configuration 2 at 180 knots and $\alpha = 17.5^\circ$
- Figure 24 Configuration 2 at 20 knots cross wind
- Figure 25 Configuration 1L at 30 knots cross wind

The Configuration 1 recovery map, Figure 21, shows a small low pressure region downstream of the lower lip during angle-of-attack operation. Figure 22 shows a large low pressure region towards the windward side at a 20 knot cross-wind condition.

The Configuration 2 recovery map, Figure 23, shows a similar low pressure region, as that of Configuration 1, at the lower lip during angle-of-attack operation. Also the low pressure region directly behind the acoustic ring can be seen in the figure. The strut wakes do not show since the rotating rake was oriented so as to avoid taking measurements directly behind the struts. Figure 24 shows the Configuration 2 inlet at a 20 knot cross-wind condition. As shown on the figure the ring provides a baffling effect, keeping the distorted low pressure flow in the outer annulus.

Figure 25 shows the Configuration 1L inlet at a 30 knot cross-wind condition. Even with the high cross flow velocity, and high inlet airflow (481 lb/sec), the low pressure region remains relatively small.

4.3.2 Pratt & Whitney Aircraft Distortion Criteria

Radial and circumferential total pressure distortion parameters and limits have been defined by Pratt & Whitney Aircraft for the JT8D-100 series engines. The distortion parameters and limits, described in Reference 4, are for instantaneous total pressures. The radial distortion limit of Reference 4 has since been updated to the limit shown in this document. The parameters are defined as:

- Radial Distortion =

$$\frac{P_{T \text{ Max Ring Avg}} - P_{T \text{ Local Ring Avg}}}{P_{T \text{ Max Ring Avg}}}$$

where ring averages are taken over a full 360°

- Circumferential Distortion =

$$\frac{P_{T \text{ Ring Avg}} - P_{T \text{ Min Sector Avg}}}{P_{T \text{ Ring Avg}}}$$

where ring averages are taken over a full 360° and Min Sector Avg is the lowest average total pressure at a given radius for the sector of concern (either a 60 degree or 180 degree sector).

During this test only steady-state total pressure measurements were taken, consequently the radial and circumferential distortion data presented are based on steady-state values only.

Distortion values were computed from the data based on the Pratt & Whitney Aircraft definitions and are presented for the following conditions:

- Figures 26, 27 and 28 - Configuration 1, 60 degree circumferential, 180 degree circumferential, and radial at static, forward speed, and angle-of-attack conditions.
- Figures 29, 30 and 31 - Configuration 1, 60 degree circumferential, 180 degree circumferential, and radial at cross-wind conditions.
- Figures 32, 33 and 34 - Configuration 2, 60 degree circumferential, 180 degree circumferential, and radial at static, forward speed, and angle-of-attack conditions.
- Figures 35, 36 and 37 - Configuration 2, 60 degrees circumferential, 180 degree circumferential, and radial at cross-wind conditions.

Figures 38, 39 and 40 - Configuration 1L, 60 degrees circumferential, 180 degree circumferential, and radial at static and cross-wind conditions.

The Configuration 1 inlet distortion falls well below the limit line at static, forward speed, and angle-of-attack conditions as shown in Figures 26, 27, and 28. This is true even for the 30 knot cross-wind 70 knot forward speed (cross wind/rolling takeoff) condition. The steady-state distortion is so low that even if a dynamic component were measured and an instantaneous distortion value computed it is expected that the distortion would remain below the limit. This is also the case for the 11 knot cross-wind condition shown on Figures 29, 30 and 31. At 20 knots cross wind the 60 degree sector distortion surpasses the limit as shown on Figure 29. The 180 degree and radial distortions fall below the limit line as shown on Figures 30 and 31.

The Configuration 2 inlet distortion, with the exception of the region directly behind the ring (probes 7, 8 and 9), falls well below the limit lines at static, forward speed, and angle-of-attack conditions as shown on Figures 32, 33 and 34. This is expected to be true even if the dynamic component were considered. The ring wake may be excluded from the limits shown, and when the limit is exceeded specific distortion patterns will be submitted to Pratt & Whitney Aircraft for evaluation (Reference 4). The circumferential distortion behind the ring shown on Figures 32 and 33 is more a measure of the asymmetry of the rotating rake and the ring rather than a true distortion. For the same reason the Figure 34 radial distortion behind the ring will be somewhat larger than that shown. For example the traverse data of Figure 18 (run 30.5) indicates a radial distortion directly behind the ring of 12 percent. Whereas, the rotating rake data of Figure 34 (run 36.5) indicates a radial distortion of 10.8 percent directly behind the ring (probe 8).

The Configuration 2 inlet, unlike Configuration 1, falls below the limit line at 20 knots cross wind as shown in Figures 35, 36 and 37 (run 15.3). The 60 degree sector distortion is near the limit line and if the dynamic component were accounted for it may surpass the limit. The 10 knot cross-wind data shown on the figures (run 14.3) falls well below the limit and if the dynamic component were considered it is expected that it would remain below the limit. As with the pressure recovery an improvement was obtained in the distortion at cross-wind conditions with the fuselage as shown in the figures.

The Configuration 1L inlet falls well below the distortion limit even up to 30 knots cross wind as shown in Figures 38, 39 and 40. Even with a dynamic component it is expected that it will fall well below the limit.

4.4 COMPARISON WITH EXISTING 727 SIDE INLET

4.4.1 Inlet Geometry and Airflow

The JT8D-100 inlet was designed to give internal performance similar to the production inlet. Consequently many of the design features are the same. Figure 41 compares the JT8D-100 inlet with the production inlet on a JT8D-15 engine. Depending on which basic JT8D engine is considered, the JT8D-100 inlet provided 40 to 48 percent more airflow and is consequently larger in diameter. The lip contraction ratios of the two inlets and cruise throat Mach number (when compared to the JT8D-1 and -7) are the same. Because of galley door access interference problems the JT8D-100 inlet was limited to 40 inches in length. This is adequate for good internal performance but limits the surface area available for acoustic treatment.

The production inlet has 4° of turning between the engine face and highlight. The JT8D-100 is axially symmetric.

4.4.2 Total Pressure Recovery

A comparison between the total pressure recovery of the production and the JT8D-100 inlets is shown on Figure 42. The production data were taken in the same tunnel facility, for approximately the same model scale (0.3 compared to 0.37), with comparable engine face probe placement and data reduction. The data presented for the production inlet is for a slightly modified model. The modifications consisted of the cowl diffuser surface being dished out somewhat, to accommodate acoustic rings in subsequent testing, and a longer centerbody. As shown in Figure 42 the JT8D-100 Configuration 1 inlet has a slightly higher recovery, at zero and 17.5 degrees angle of attack at cruise airflows, than the modified production model. The Configuration 2 recovery is slightly lower (.003) than the Configuration 1 inlet at the cruise airflow.

4.4.3 Total Pressure Distortion

A comparison of the total pressure distortion for the JT8D-100, the modified production, and the full scale production inlet is shown in Figure 43. The distortion parameter, shown in the figure, is for the (average-minimum)/average total pressure ratio which has been used in past inlet development testing. As shown in the figure the Configuration 1 model distortion is lower than that of the modified production inlet.

5.0 CONCLUSIONS

The cruise and angle-of-attack recovery and distortion of the hardwall Configuration 1 inlet will be slightly better than that of the existing 727 hardwall inlet. Since the new 727 inlet utilizes a maximum of peripheral treatment the same statement will be true when acoustic treatment is included for both inlets. The hardwall Configuration 2 cruise recovery will be slightly lower (0.003) than that of the Configuration 1 inlet.

The Configuration 1 and 2 inlets have an acceptable distortion at 11 knots cross wind, but the distortion becomes marginal when compared to the Pratt & Whitney Aircraft limit at 20 knots cross wind. The 30 knot cross-wind condition at 70 knots forward speed (cross-wind/rolling takeoff) shows an acceptable distortion level. The two inlets were designed using a throat Mach number and lip contour that give an equivalent or slightly better cross-wind performance than the existing 727, and using normal operating procedures cross-wind performance should not present a problem. For a small cruise performance penalty, Configuration 1L will provide additional static cross-wind capability (up to 30 knots).

The acoustic ring of Configuration 2 provides a baffling effect, when compared to Configuration 1, keeping the low pressure distorted flow in the outer annulus. This results in a "clean" core flow at all test conditions.

The Configuration 2R inlet showed that the ring leading edge may be moved further into the throat, thus providing more acoustic treatment area, without a static, cross-wind, or angle-of-attack recovery or distortion penalty.

6.0 FIGURES

<u>Figure No.</u>	<u>Title</u>	<u>Page</u>
1	CONFIGURATIONS 1 AND 2 JT8D-100 SIDE INLET	30
2	CONFIGURATION 2 PREDICTED MACH NUMBER DISTRIBUTION	31
3	CONFIGURATIONS 1 AND 2 SURFACE MACH NUMBER DISTRIBUTION (Potential Flow Analysis)	32
4	CONFIGURATIONS 1 AND 2 AREA DISTRIBUTION AND MACH NUMBER	33
5	SIDE INLET TEST CONFIGURATIONS	34
6	CROSS-WIND INSTALLATION	35
7	CONFIGURATION 2 FORWARD SPEED INSTALLATION	35
8	INLET CONFIGURATION 2	35
9	WIND TUNNEL CROSS-WIND AND FORWARD SPEED INSTALLATIONS	36
10	CONFIGURATIONS 1 AND 2 STATIC PRESSURE PORT LOCATIONS	37
11	ROTATING RAKE CONFIGURATION	38
12	CONFIGURATION 1 SURFACE MACH NUMBER DISTRIBUTIONS	39
13	CONFIGURATION 2 SURFACE MACH NUMBER DISTRIBUTIONS	40
14	CONFIGURATION 1 PRESSURE RECOVERY VS AIRFLOW (Static & Cross-Wind Conditions)	41
15	CONFIGURATION 1 PRESSURE RECOVERY VS AIRFLOW (Static, Fwd Speed and Angle-of-Attack Conditions)	42
16	CONFIGURATION 2 PRESSURE RECOVERY VS AIRFLOW (Static and Cross-Wind Conditions)	43

Preceding page blank

<u>Figure No.</u>	<u>Title</u>	<u>Page</u>
17	CONFIGURATION 2 PRESSURE RECOVERY VS AIR-FLOW (Static, Fwd Speed and Angle-of-Attack Conditions)	44
18	CONFIGURATION 2 ENGINE FACE RING AND STRUT TOTAL PRESSURE TRAVERSE	45
19	CONFIGURATION 1L PRESSURE RECOVERY VS AIRFLOW (Static & Cross-Wind Conditions)	46
20	CONFIGURATION 2R PRESSURE RECOVERY VS AIR-FLOW (Static, Angle-of-Attack and Cross-Wind Conditions)	47
21	CONFIGURATION 1 ENGINE FACE PRESSURE RECOVERY MAP (180 Knots @ $\alpha = 17.5^\circ$)	48
22	CONFIGURATION 1 ENGINE FACE PRESSURE RECOVERY MAP (20 Knots Cross Wind)	49
23	CONFIGURATION 2 ENGINE FACE PRESSURE RECOVERY MAP (180 Knots @ $\alpha = 17.5^\circ$)	50
24	CONFIGURATION 2 ENGINE FACE PRESSURE RECOVERY MAP (20 Knots Cross-Wind)	51
25	CONFIGURATION 1L ENGINE FACE PRESSURE RECOVERY MAP (30 Knots Cross-wind)	52
26	CONFIGURATION 1 CIRCUMFERENTIAL PRESSURE DISTORTION 60° SECTOR (Static, Fwd Speed and Angle-of-Attack Conditions)	53
27	CONFIGURATION 1 CIRCUMFERENTIAL PRESSURE DISTORTION 180° SECTOR (Static, Fwd Speed and Angle-of-Attack Conditions)	54
28	CONFIGURATION 1 RADIAL PRESSURE DISTORTION (Static, Fwd Speed and Angle-of-Attack Conditions)	55
29	CONFIGURATION 1 CIRCUMFERENTIAL PRESSURE DISTORTION 60° SECTOR (Cross-Wind Conditions)	56
30	CONFIGURATION 1 CIRCUMFERENTIAL PRESSURE DISTORTION 180° SECTOR (Cross-Wind Conditions)	57

<u>Figure No.</u>	<u>Title</u>	<u>Page</u>
31	CONFIGURATION 1 RADIAL PRESSURE DISTORTION (Cross-Wind Conditions)	58
32	CONFIGURATION 2 CIRCUMFERENTIAL PRESSURE DISTORTION 60° SECTOR (Static, Fwd Speed and Angle-of-Attack Conditions)	59
33	CONFIGURATION 2 CIRCUMFERENTIAL PRESSURE DISTORTION 180° SECTOR (Static, Fwd Speed and Angle-of-Attack Conditions)	60
34	CONFIGURATION 2 RADIAL PRESSURE DISTORTION (Static, Fwd Speed and Angle-of-Attack Conditions)	61
35	CONFIGURATION 2 CIRCUMFERENTIAL PRESSURE DISTORTION 60° SECTOR (Static and Cross- Wind Conditions)	62
36	CONFIGURATION 2 CIRCUMFERENTIAL PRESSURE DISTORTION 180° SECTOR (Static and Cross-Wind Conditions)	63
37	CONFIGURATION 2 RADIAL PRESSURE DISTORTION (Static and Cross-Wind Conditions)	64
38	CONFIGURATION 1L CIRCUMFERENTIAL PRESSURE DISTORTION 60° SECTOR (Static and Cross- Wind Conditions)	65
39	CONFIGURATION 1L CIRCUMFERENTIAL PRESSURE DISTORTION 180° SECTOR (Static and Cross- Wind Conditions)	66
40	CONFIGURATION 1L RADIAL PRESSURE DISTORTION (Static and Cross-Wind Conditions)	67
41	DESIGN COMPARISON OF 727 PRODUCTION AND JT8D-100 SIDE INLETS	68
42	PRESSURE RECOVERY COMPARISON 727-200 PRODUCTION (Modified) AND JT8D-100 SIDE INLETS	69
43	TOTAL PRESSURE DISTORTION COMPARISON 727-200 PRODUCTION AND JT8D-100 SIDE INLETS	70

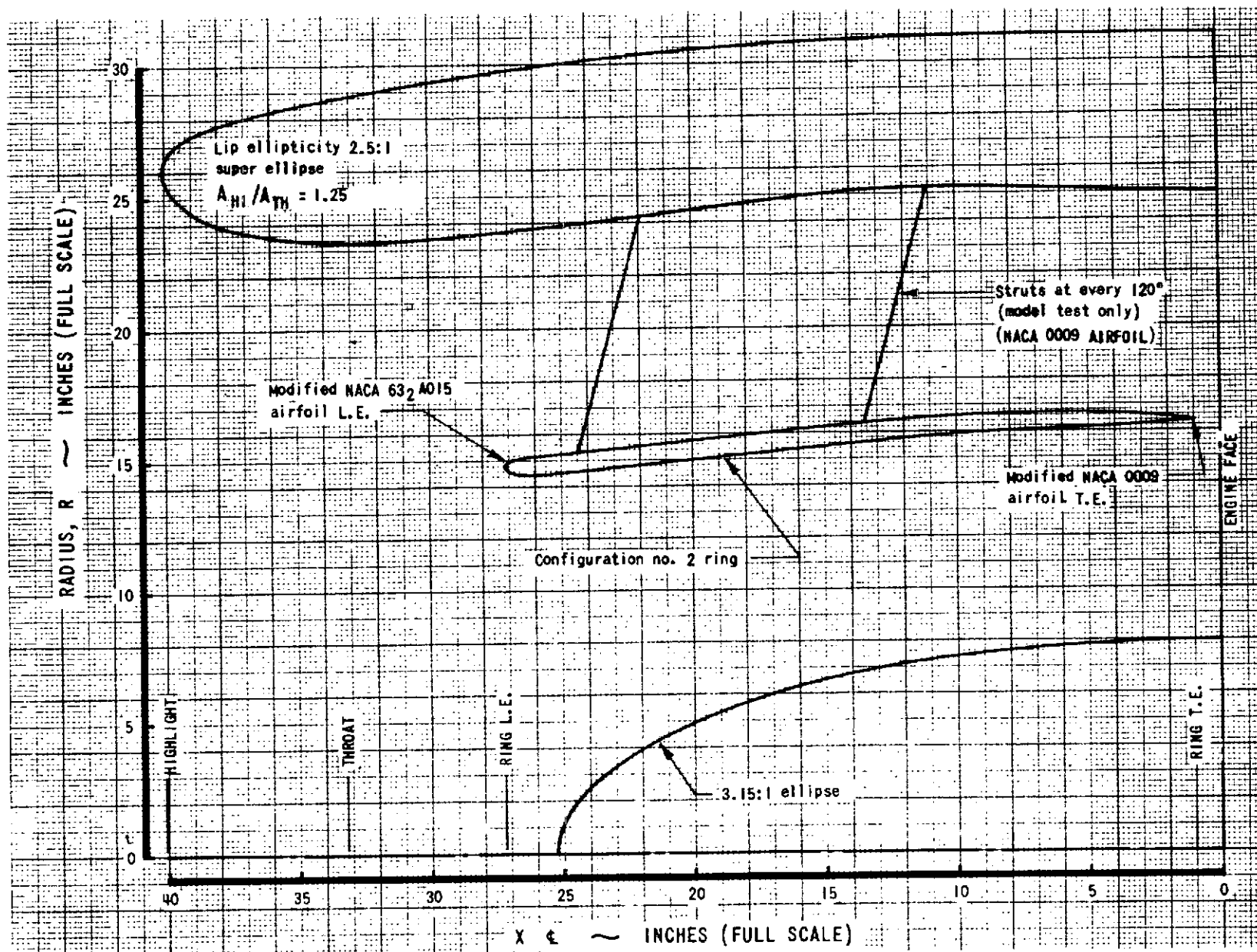


FIGURE 1 CONFIGURATIONS 1 AND 2 JT8D-100 SIDE INLET

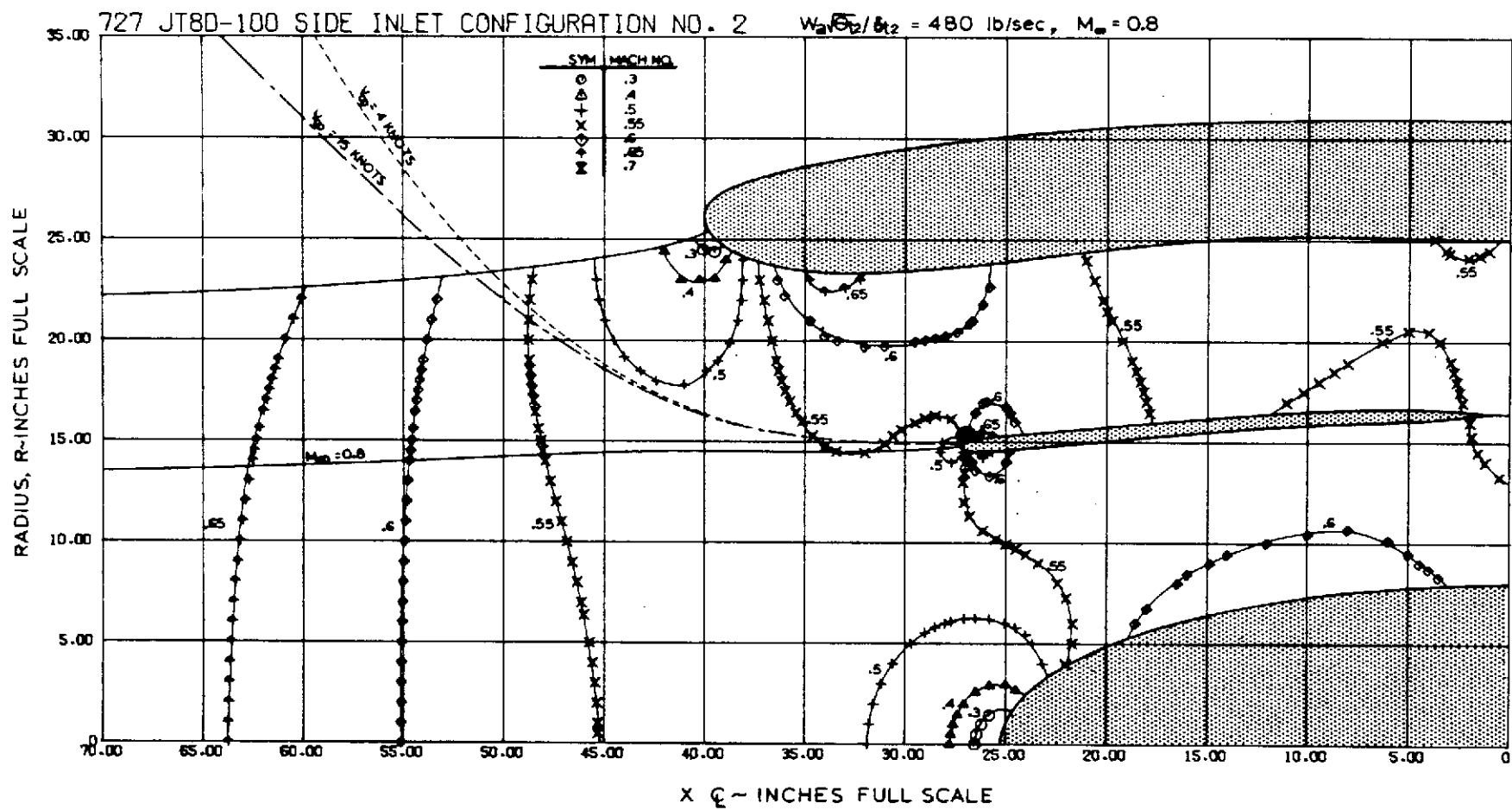


FIG 2 PREDICTED MACH NUMBER DISTRIBUTION (Configuration 2)

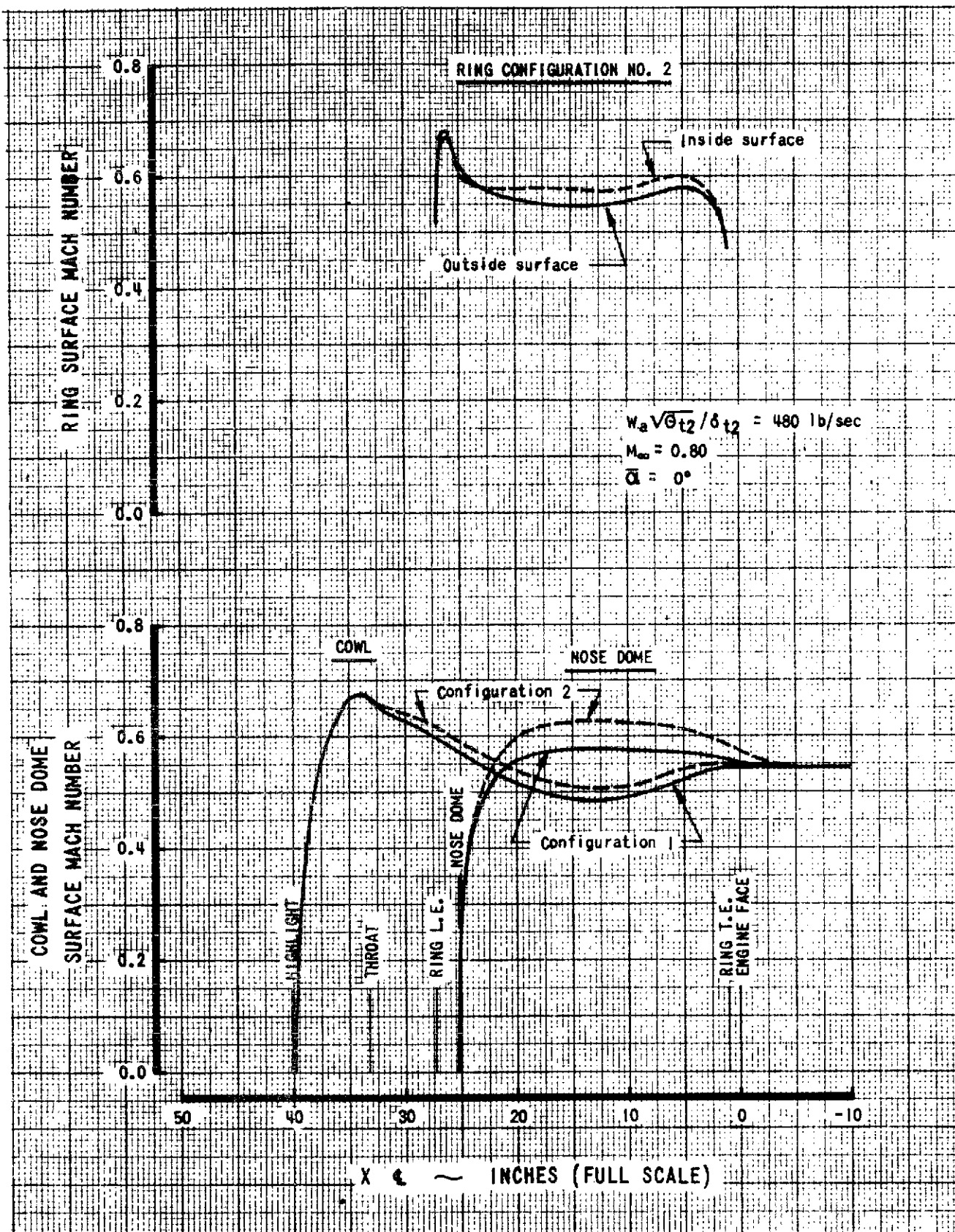


FIGURE 3 CONFIGURATIONS 1 AND 2 SURFACE MACH NUMBER DISTRIBUTION (Potential Flow Analysis)

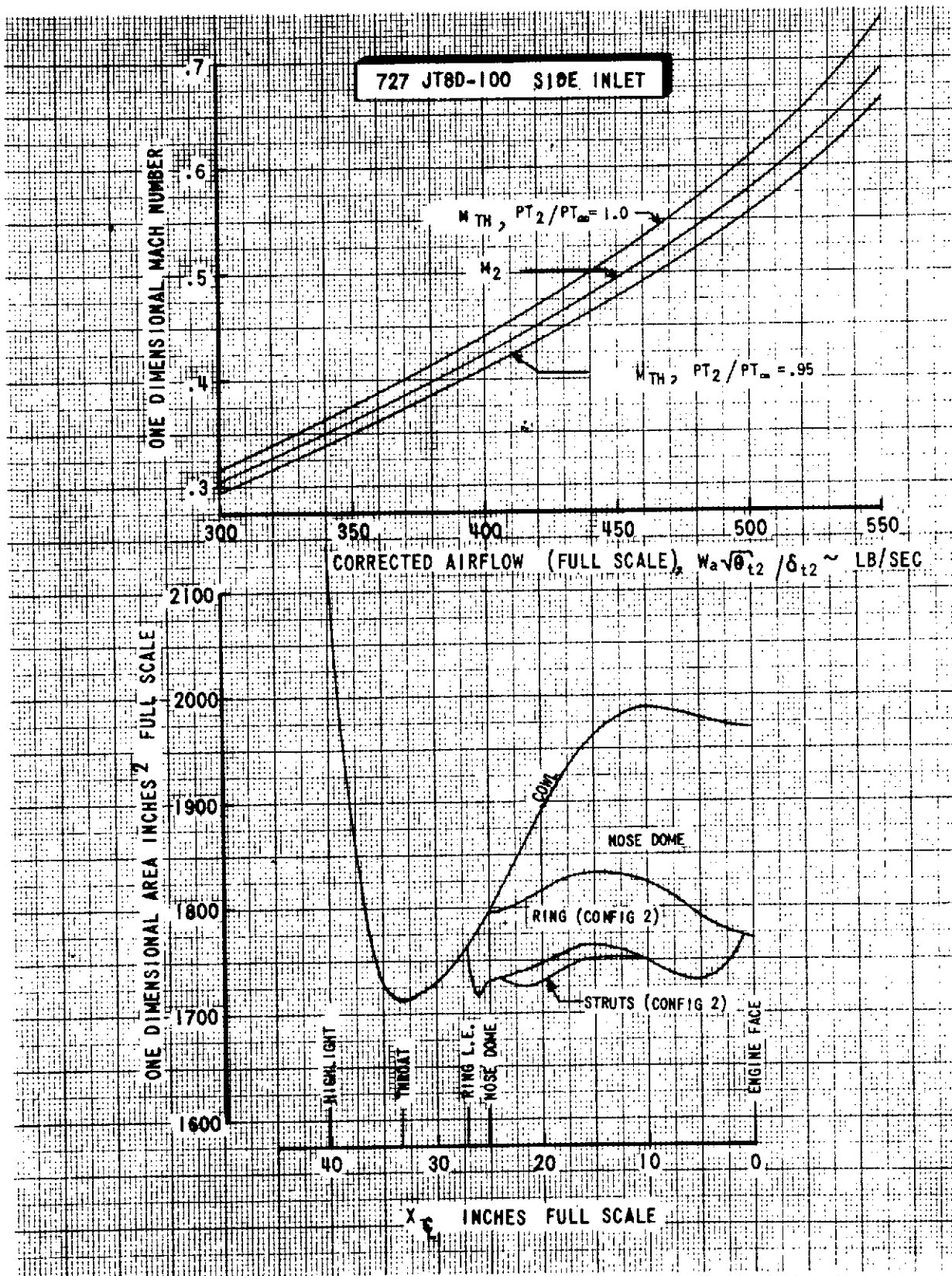
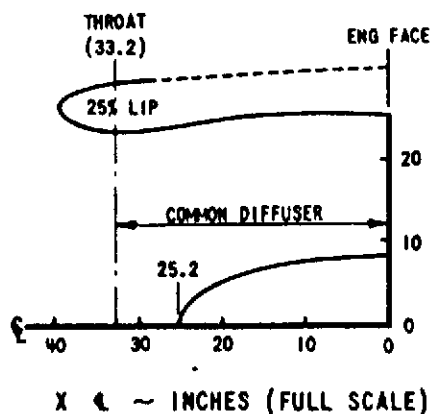
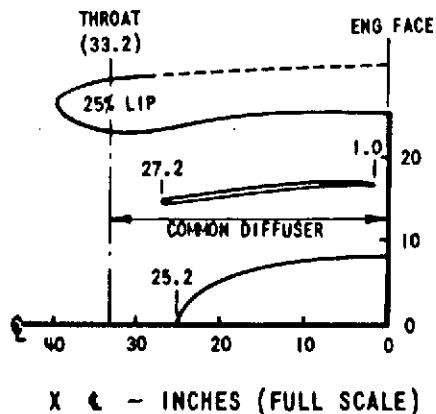


FIGURE 4 CONFIGURATIONS 1 AND 2 AREA DISTRIBUTION AND MACH NUMBER

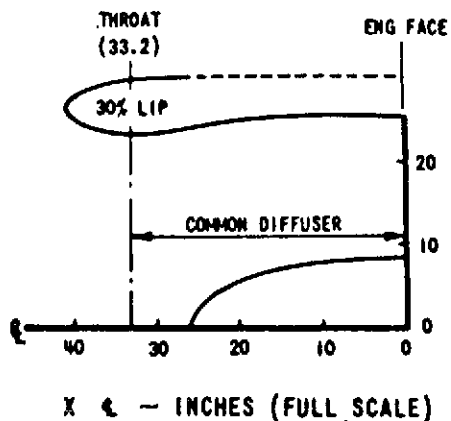
CONFIGURATION 1



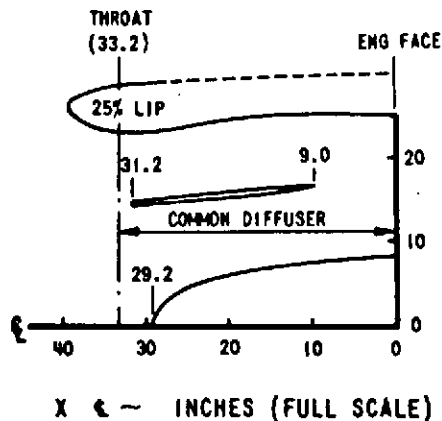
CONFIGURATION 2



CONFIGURATION 1L



CONFIGURATION 2R



Notes:

- o Throat diameter 46.70 in. (full scale) - all models.
- o Engine face cowl diameter 50.10 in. (full scale) - all models.
- o Nose dome engine face diameter 16.00 in. (full scale) - all models.
- o Common nose dome on configurations 1, 2 and 1L.
- o 25% lip defined as $A_{N1}/A_{TH} = 1.25$.

FIGURE 5 SIDE INLET TEST CONFIGURATIONS

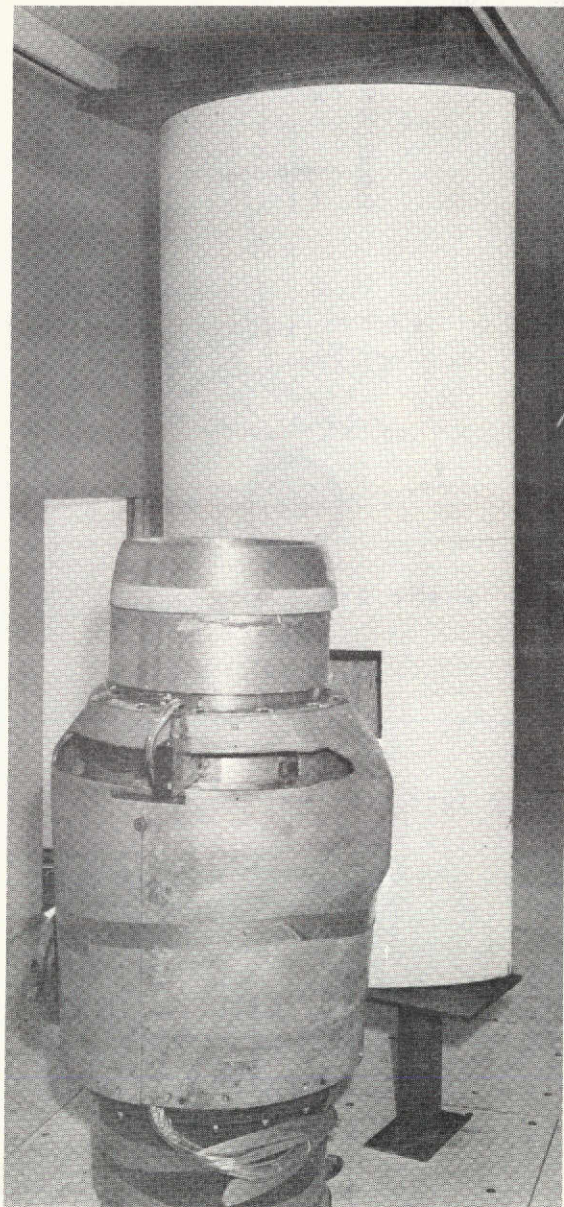


FIGURE 6 CROSS-WIND
INSTALLATION

This page is reproduced at the
back of the report by a different
reproduction method to provide
better detail.

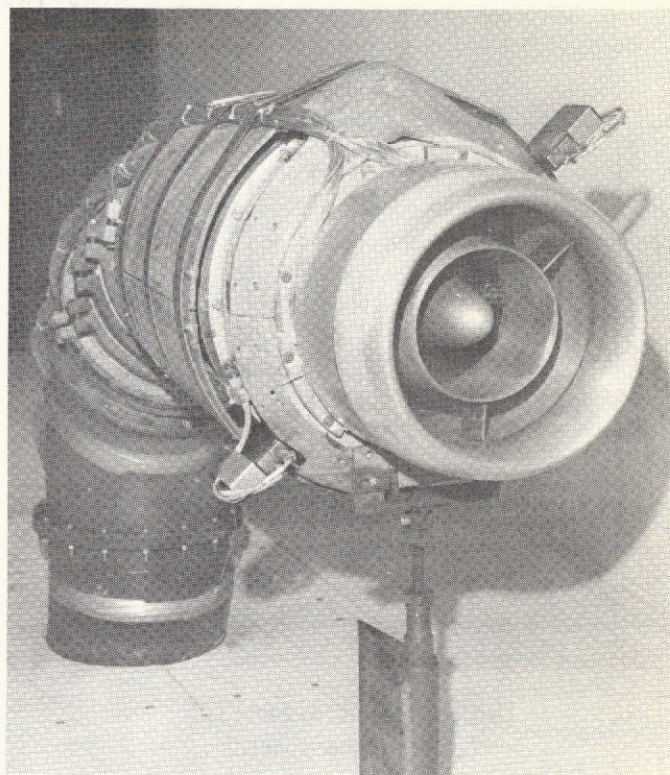


FIGURE 7 CONFIGURATION 2 FORWARD
SPEED INSTALLATION

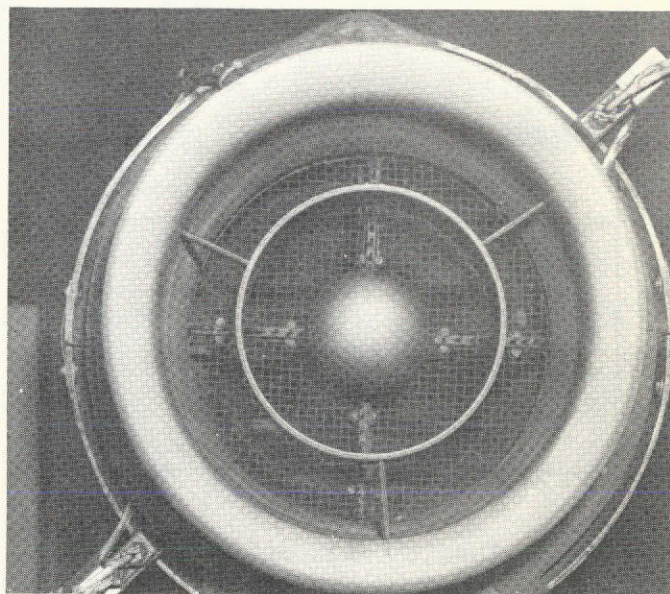
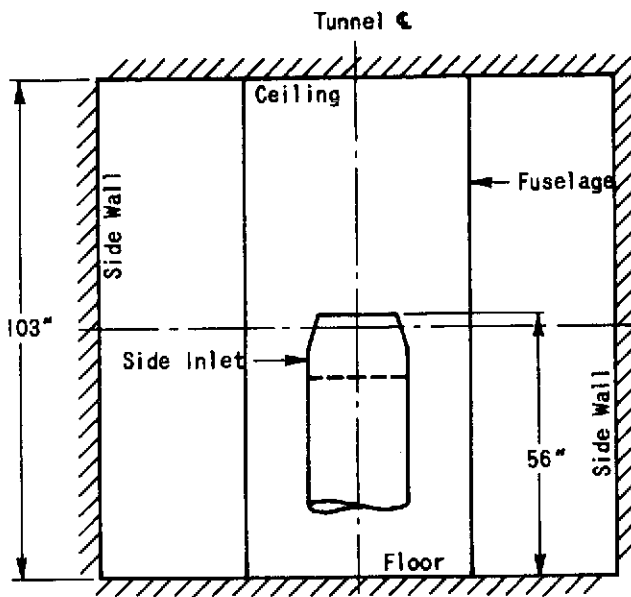
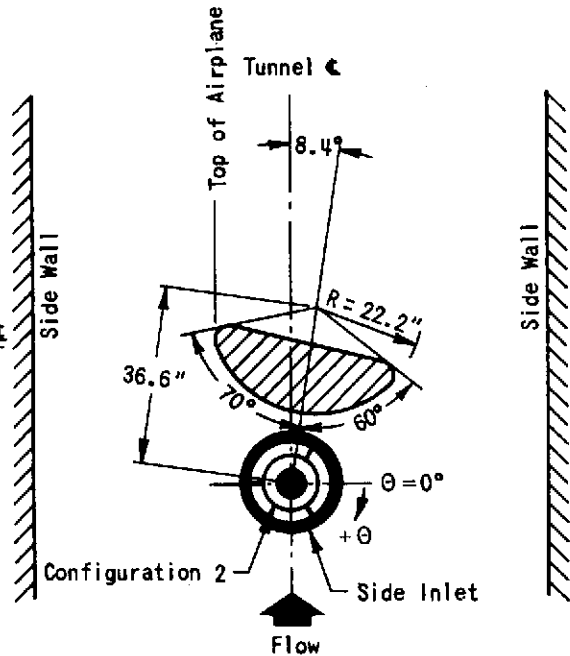


FIGURE 8 INLET CONFIGURATION 2

CROSS-WIND INSTALLATION

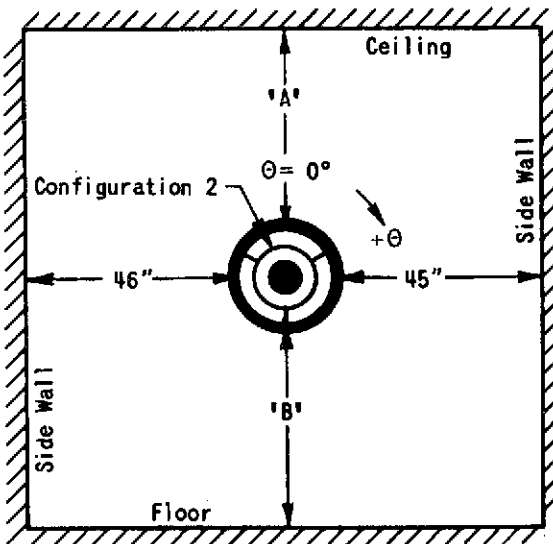


TUNNEL CROSS SECTION
(LOOKING DOWN TUNNEL)



PLAN VIEW

FORWARD SPEED ANGLE-OF-ATTACK INSTALLATION

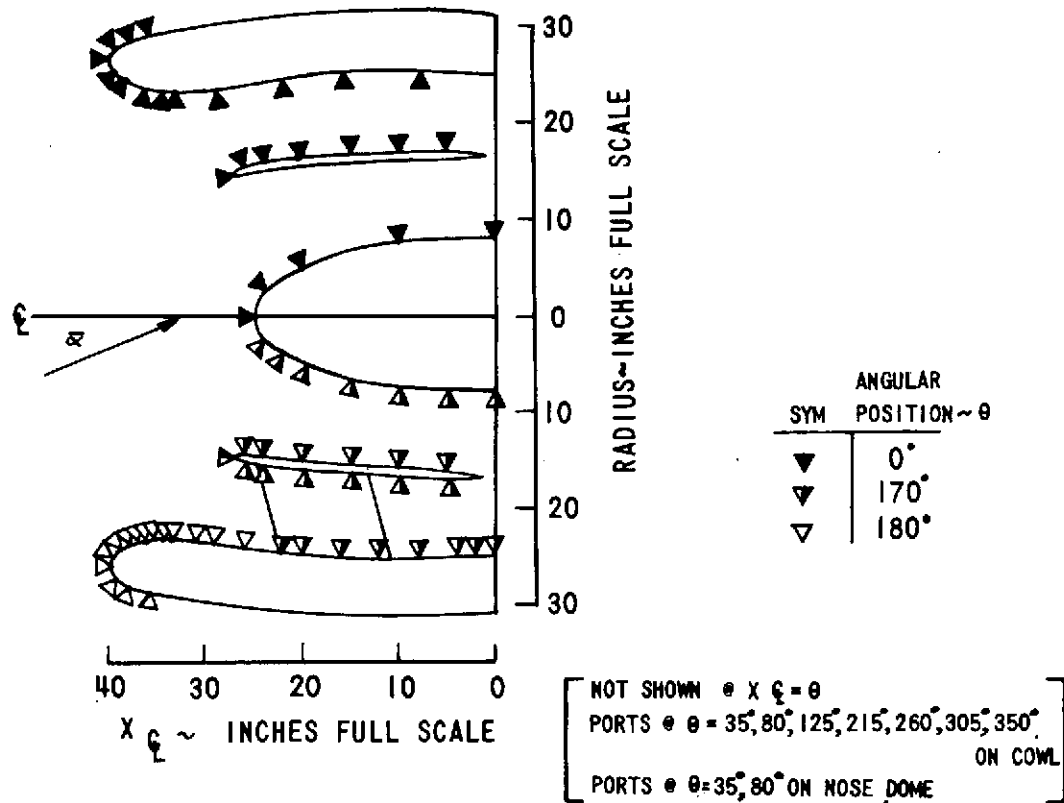


TUNNEL CROSS SECTION
(LOOKING DOWN TUNNEL)

α ~ Deg.	"A" ~ In.	"B" ~ In.
0	54.0	33.0
14.8	40.6	46.4
17.5	38.0	49.0
22.5	33.0	54.0

ALL DIMENSIONS INCHES MODEL SCALE

FIGURE 9 WIND TUNNEL CROSS-WIND AND FORWARD SPEED INSTALLATIONS



	COWL			RING		NOSE DOME		
	$X\xi$ Inches Full Scale	$\theta = 0^\circ$	$\theta = 170^\circ$	Inside $\theta = 170^\circ$	Outside $\theta = 0^\circ$	$\theta = 170^\circ$	$\theta = 0^\circ$	$\theta = 170^\circ$
	0.0		x				x	x
	2.0		x					
	4.0		x					
	5.0							
	8.0	x	x					
	10.0			x	x	x	x	x
	12.0		x					
	15.0			x	x	x		x
	16.0	x	x					
	20.0		x	x	x	x	x	x
	22.0							x
	22.4	x	x					
	24.0			x	x	x	x	x
	25.2						x	
	26.0							
	26.2			x	x	x		
	27.2			x	x			
	29.0	x						
	31.0							
	33.2	x						
	34.25	x						
	35.24							
	36.24	x						
	37.2							
	38.15							
	39.05	x						
	39.8	x						
	40.09	x						
	39.73	x						
	37.97	x						
	36.07	x						

FIGURE 10 CONFIGURATIONS 1 AND 2 STATIC PRESSURE PORT LOCATIONS

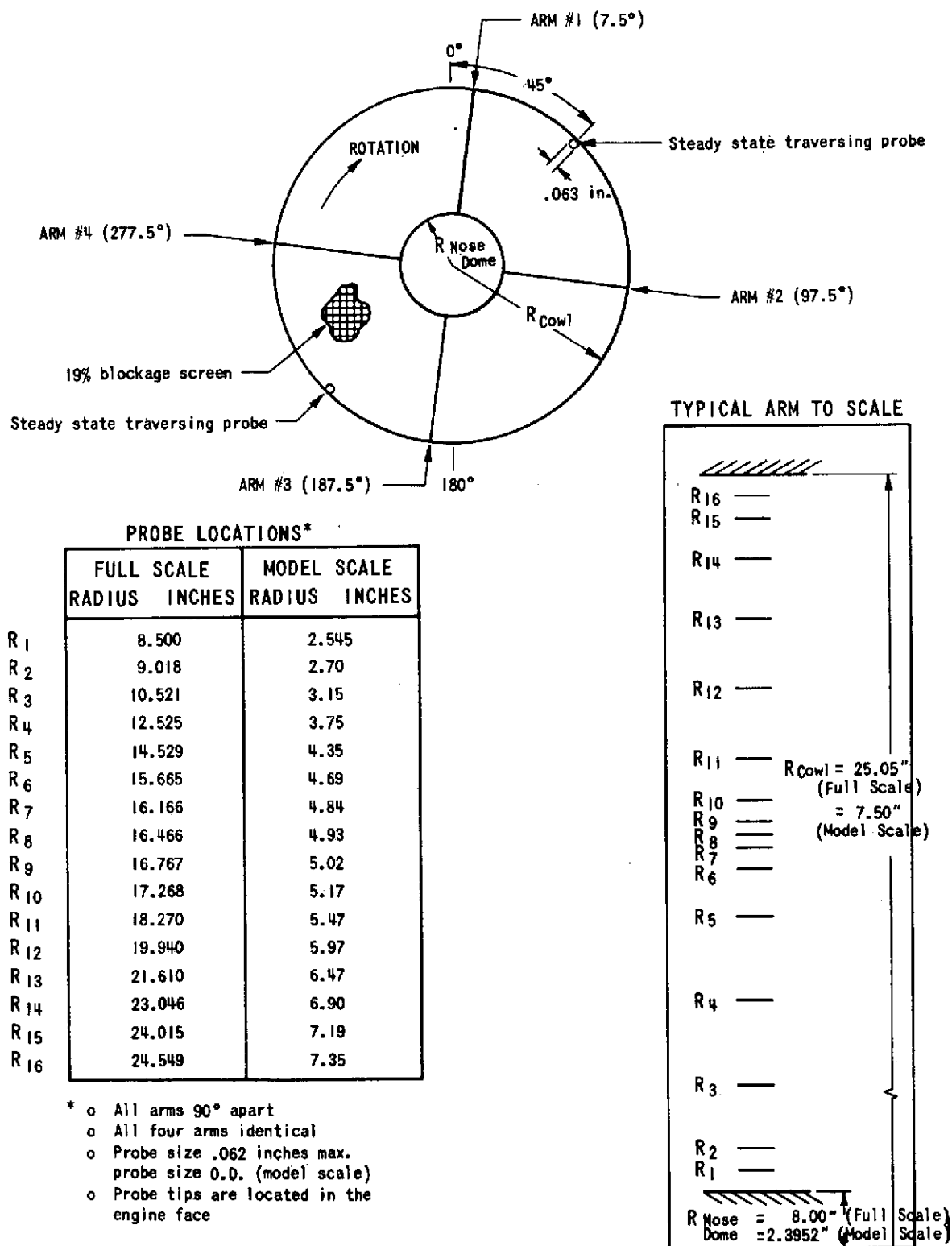


FIGURE 11 ROTATING RAKE CONFIGURATION.

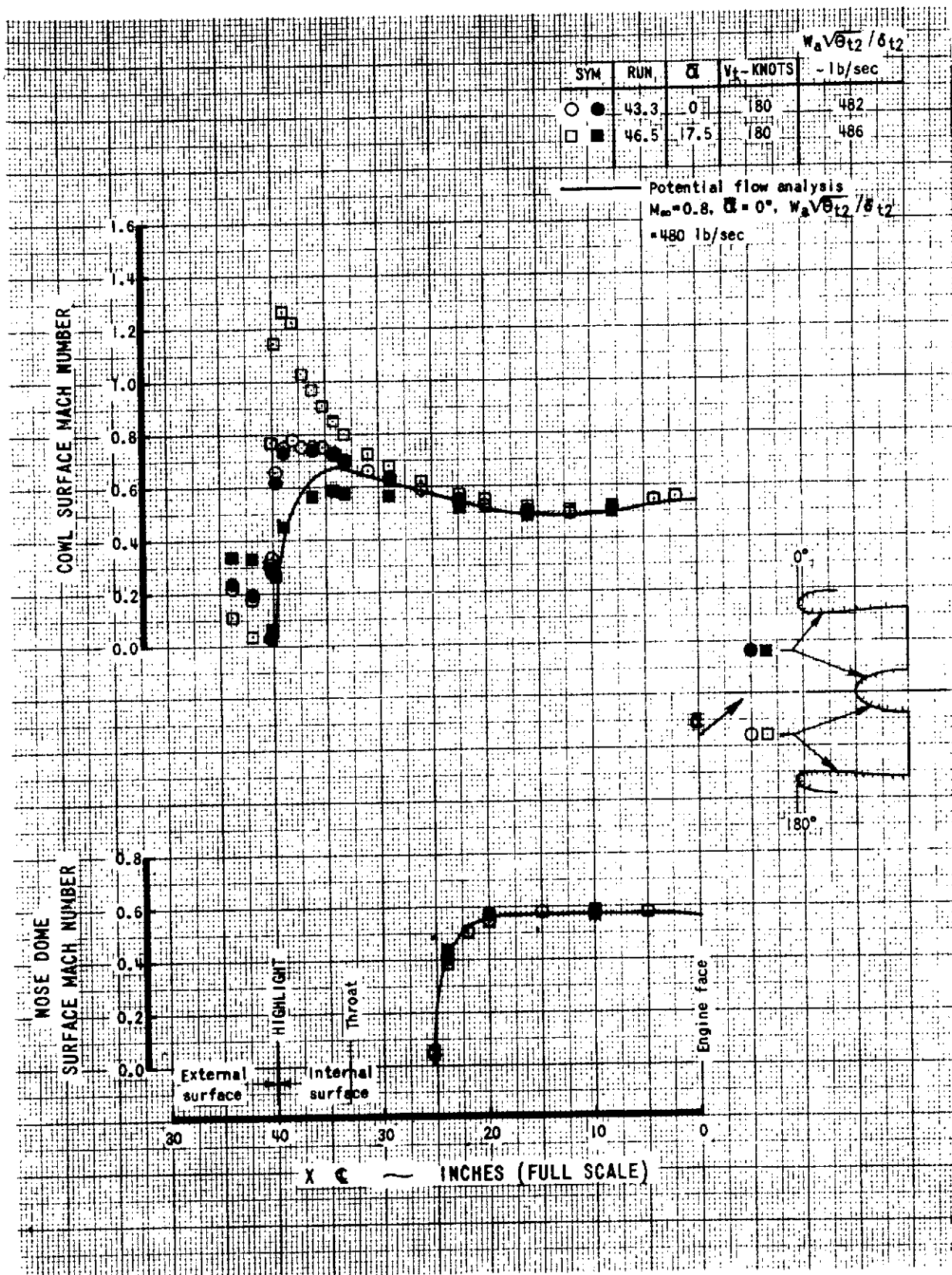


FIGURE 12 CONFIGURATION 1 SURFACE MACH NUMBER DISTRIBUTIONS

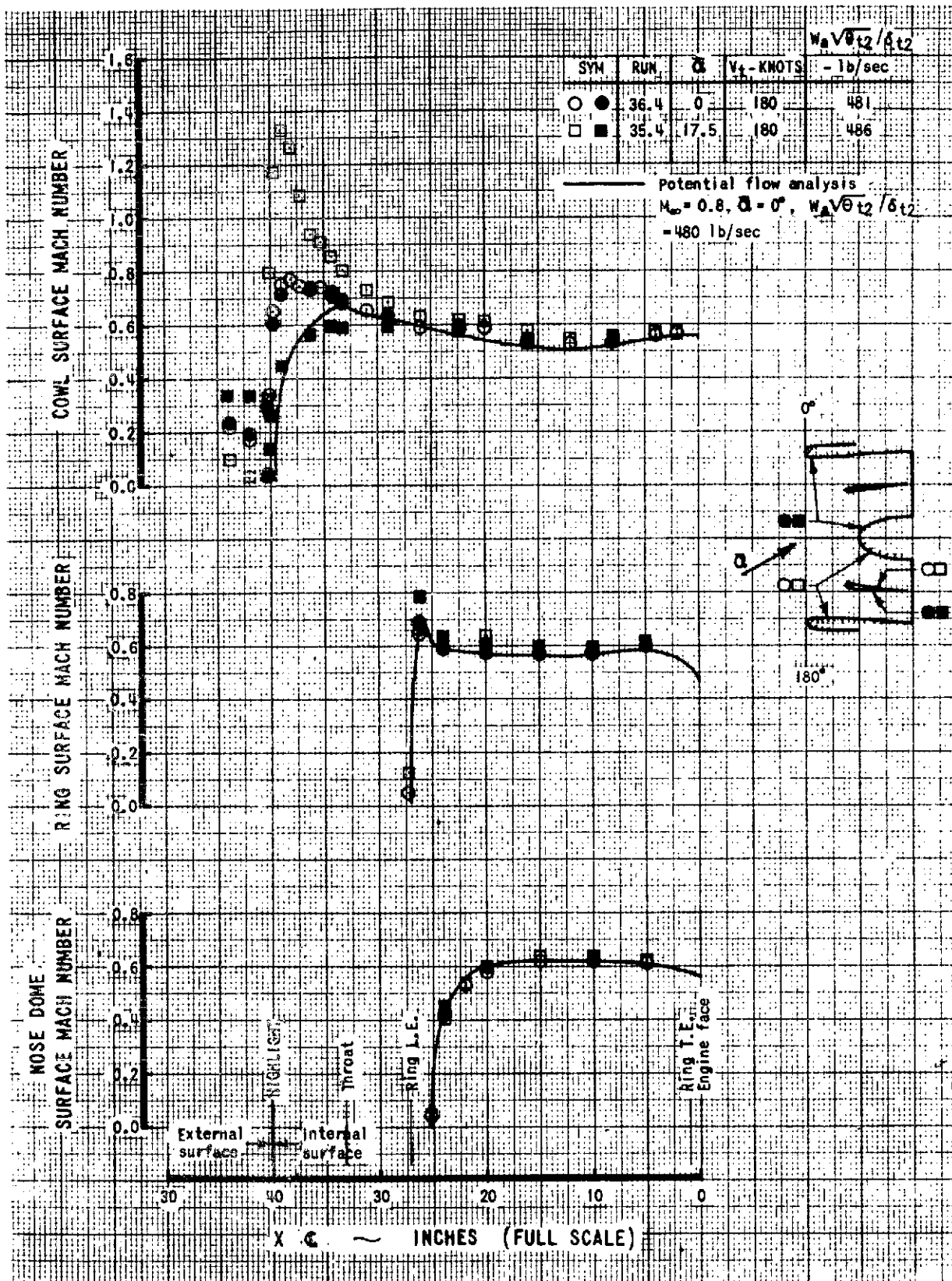


FIGURE 13 CONFIGURATION 2 SURFACE MACH NUMBER DISTRIBUTIONS

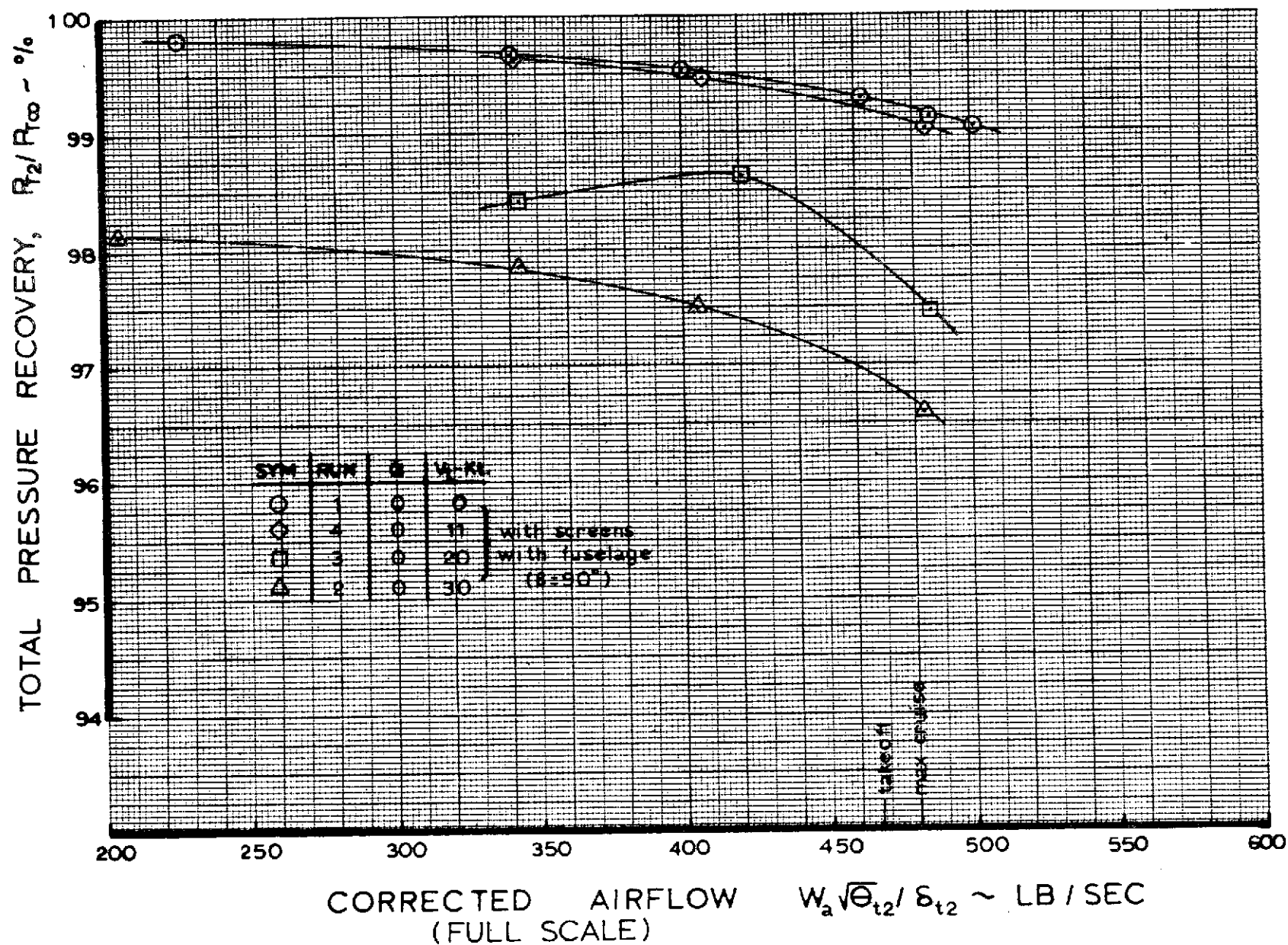


FIGURE 14 CONFIGURATION 1 PRESSURE RECOVERY VS AIRFLOW (Static & Cross-Wind Conditions)

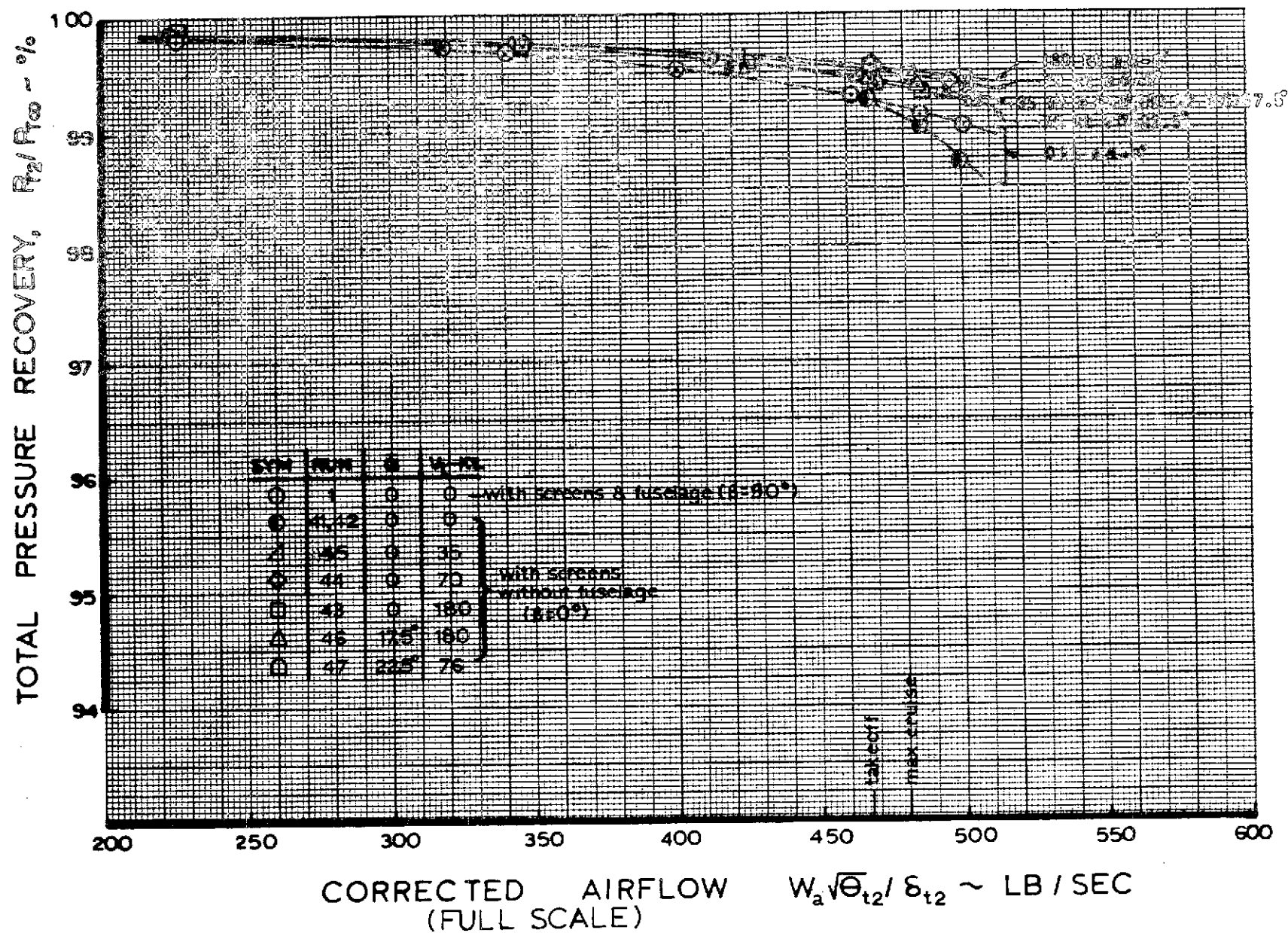


FIGURE 15 CONFIGURATION 1 PRESSURE RECOVERY VS AIRFLOW (Static, Fwd Speed and Angle-of-Attack Conditions)

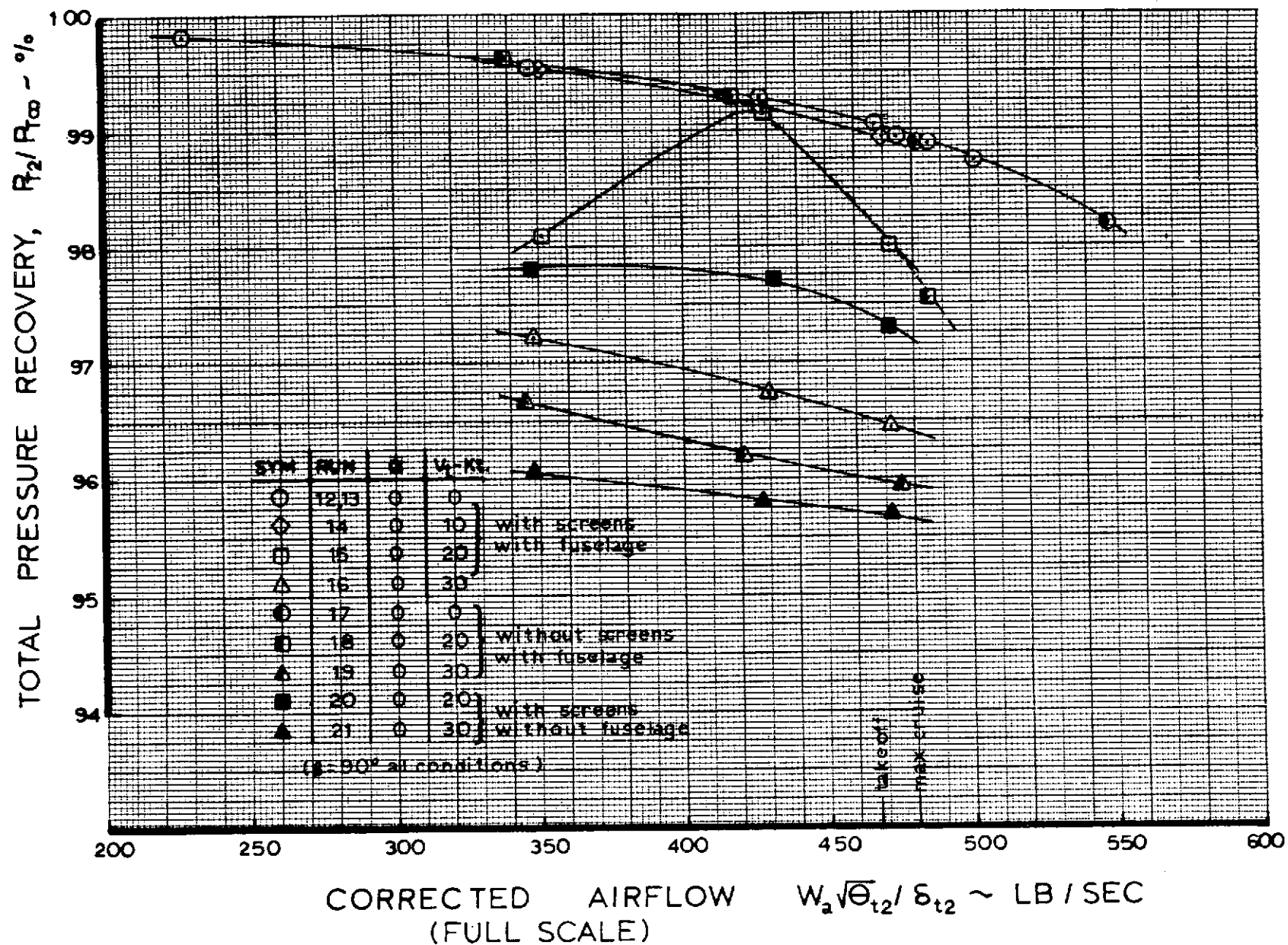


FIGURE 16 CONFIGURATION 2 PRESSURE RECOVERY VS AIRFLOW (Static and Cross-Wind Conditions)

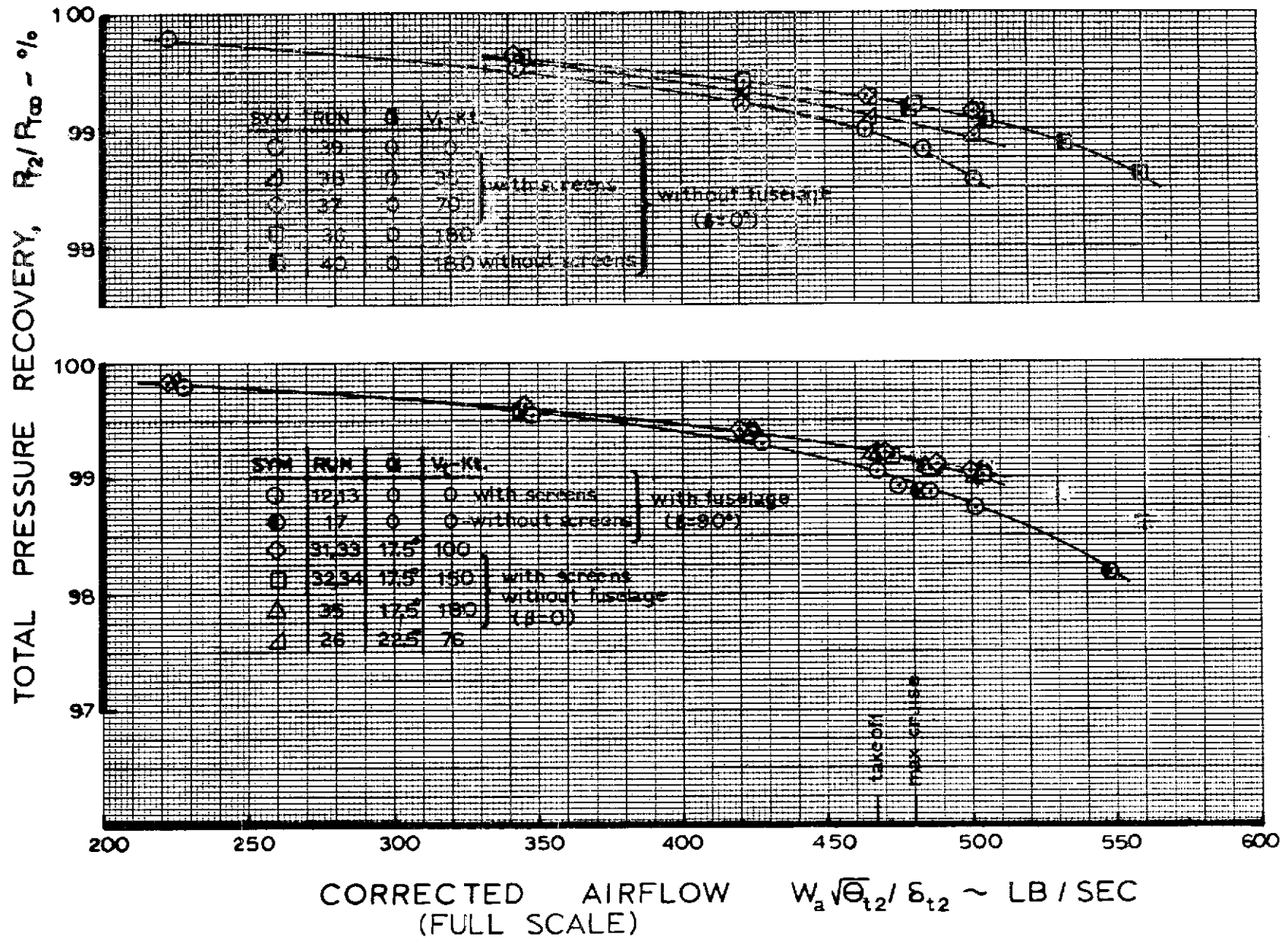


FIGURE 17 CONFIGURATION 2 PRESSURE RECOVERY VS AIRFLOW (Static, Fwd Speed and Angle-of-Attack Conditions)

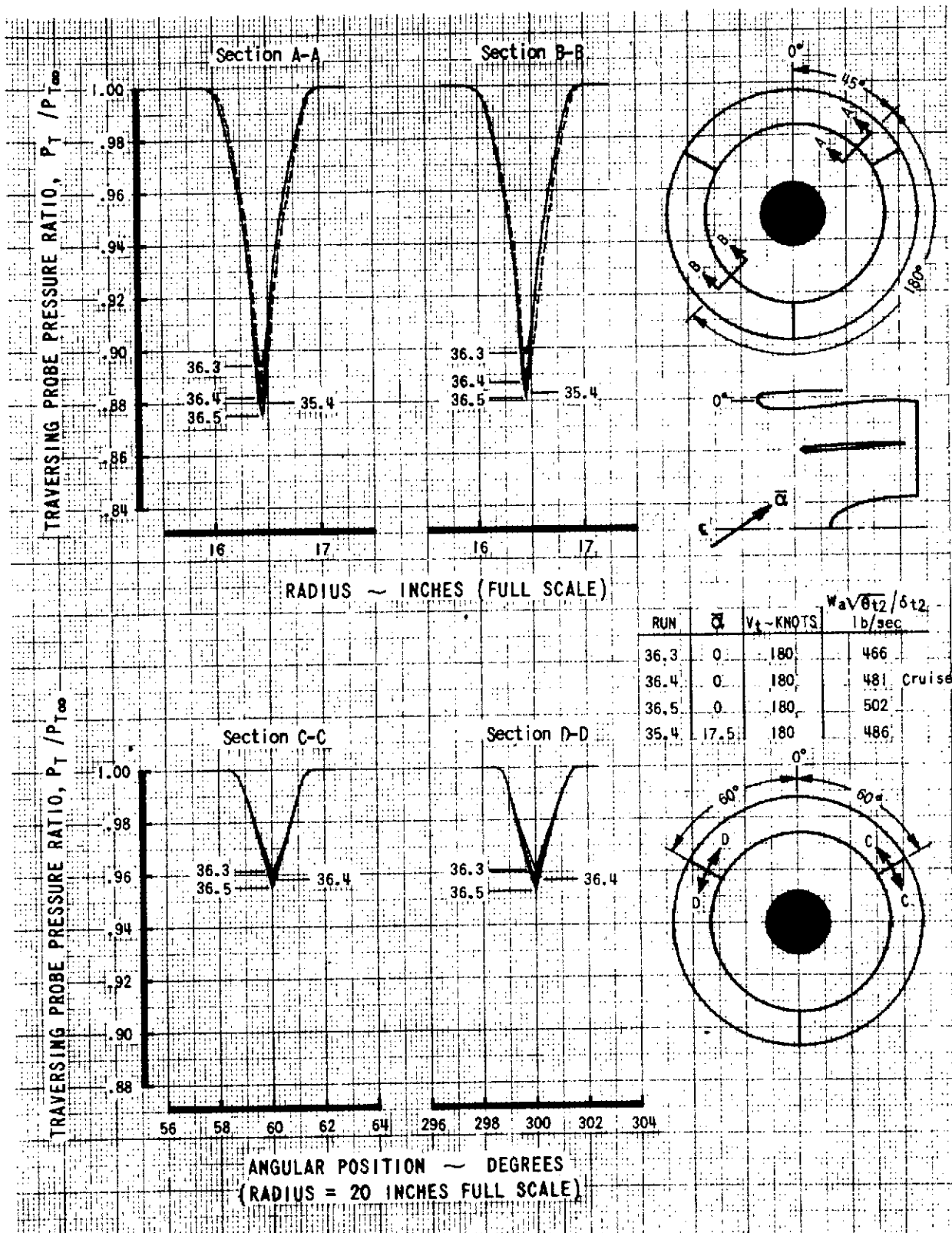


FIGURE 18 CONFIGURATION 2 ENGINE FACE RING AND STRUT
TOTAL PRESSURE TRAVERSE

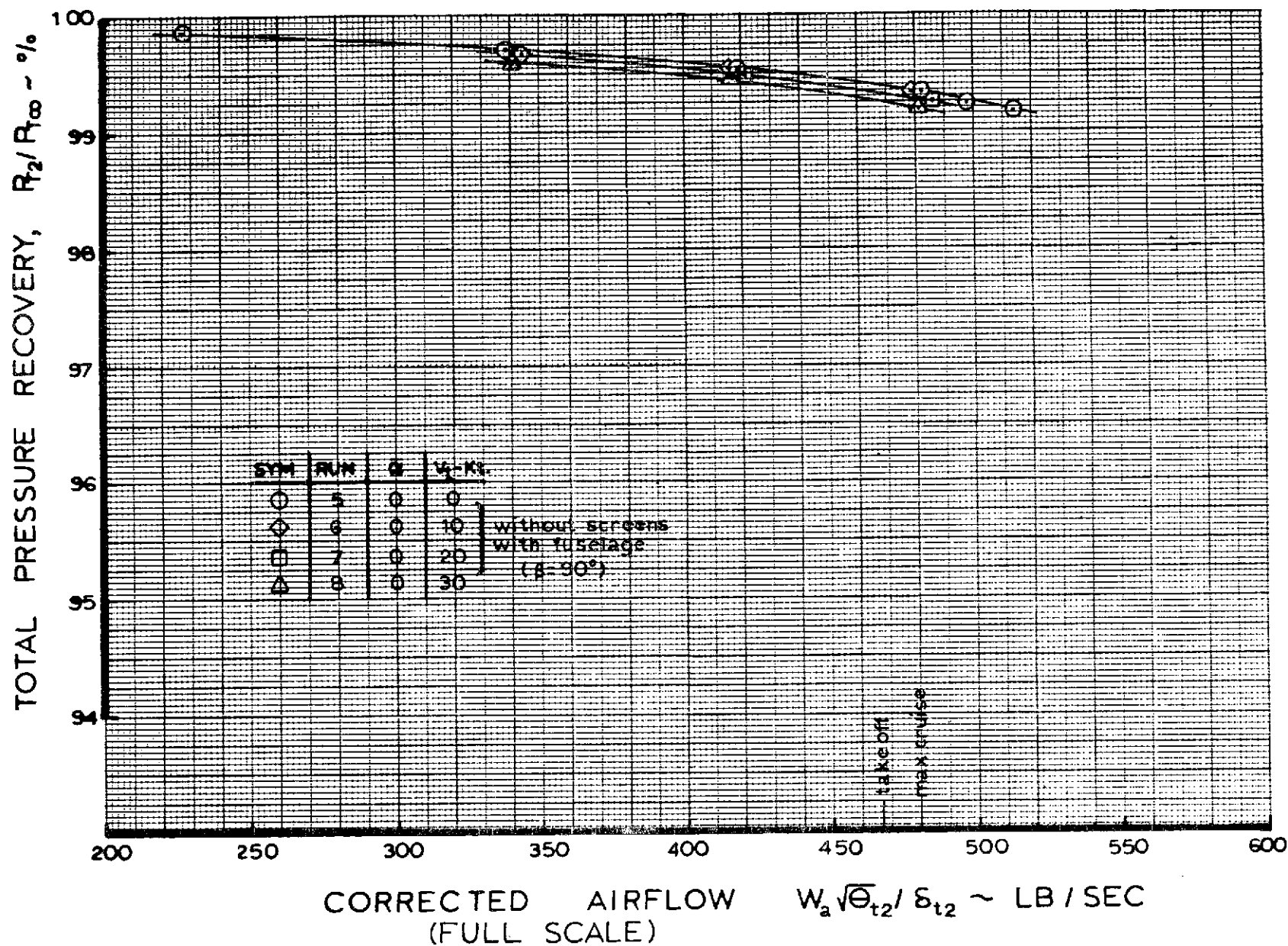


FIGURE 19 CONFIGURATION 1L PRESSURE RECOVERY VS AIRFLOW (Static & Cross-Wind Conditions)

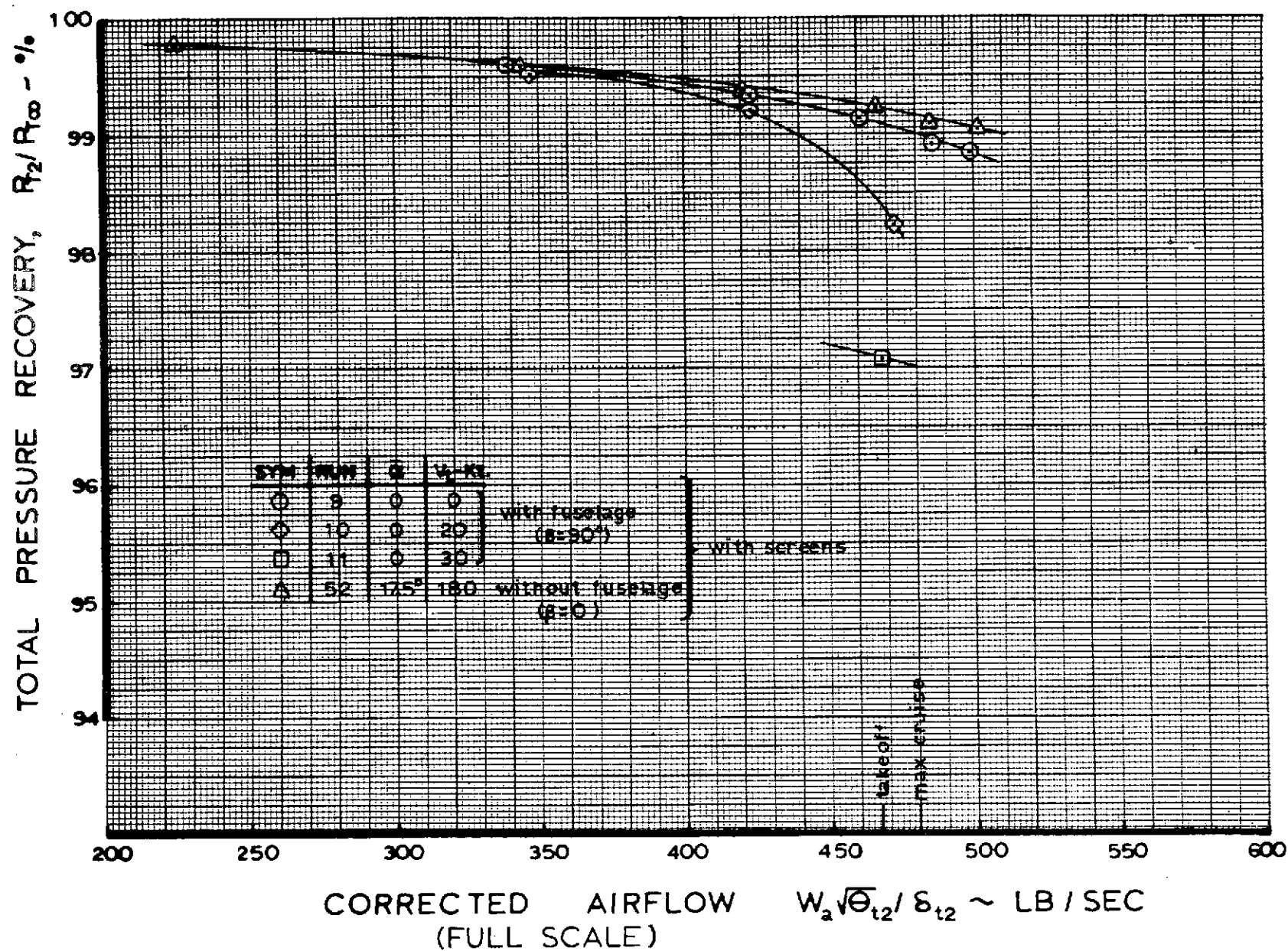
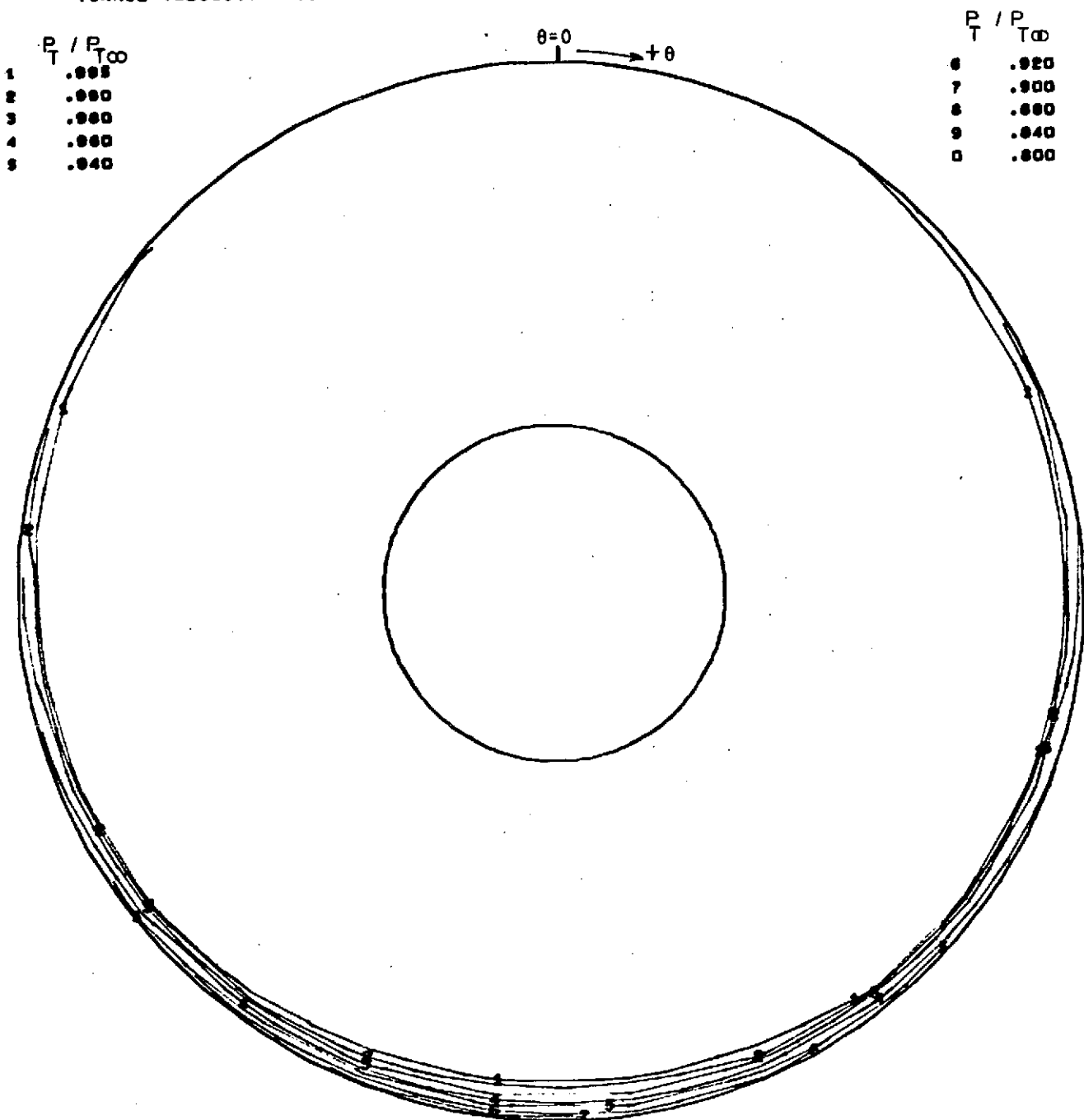


FIGURE 20 CONFIGURATION 2R PRESSURE RECOVERY VS AIRFLOW (Static, Angle-of-Attack and Cross-Wind Conditions)

727 REFAN, SIDE INLET MODEL TEST
 CONFIG. 1, ALPHA = 17.5 DEG. FWD. VELOCITY
 TUNNEL VELOCITY = 180 KNOTS



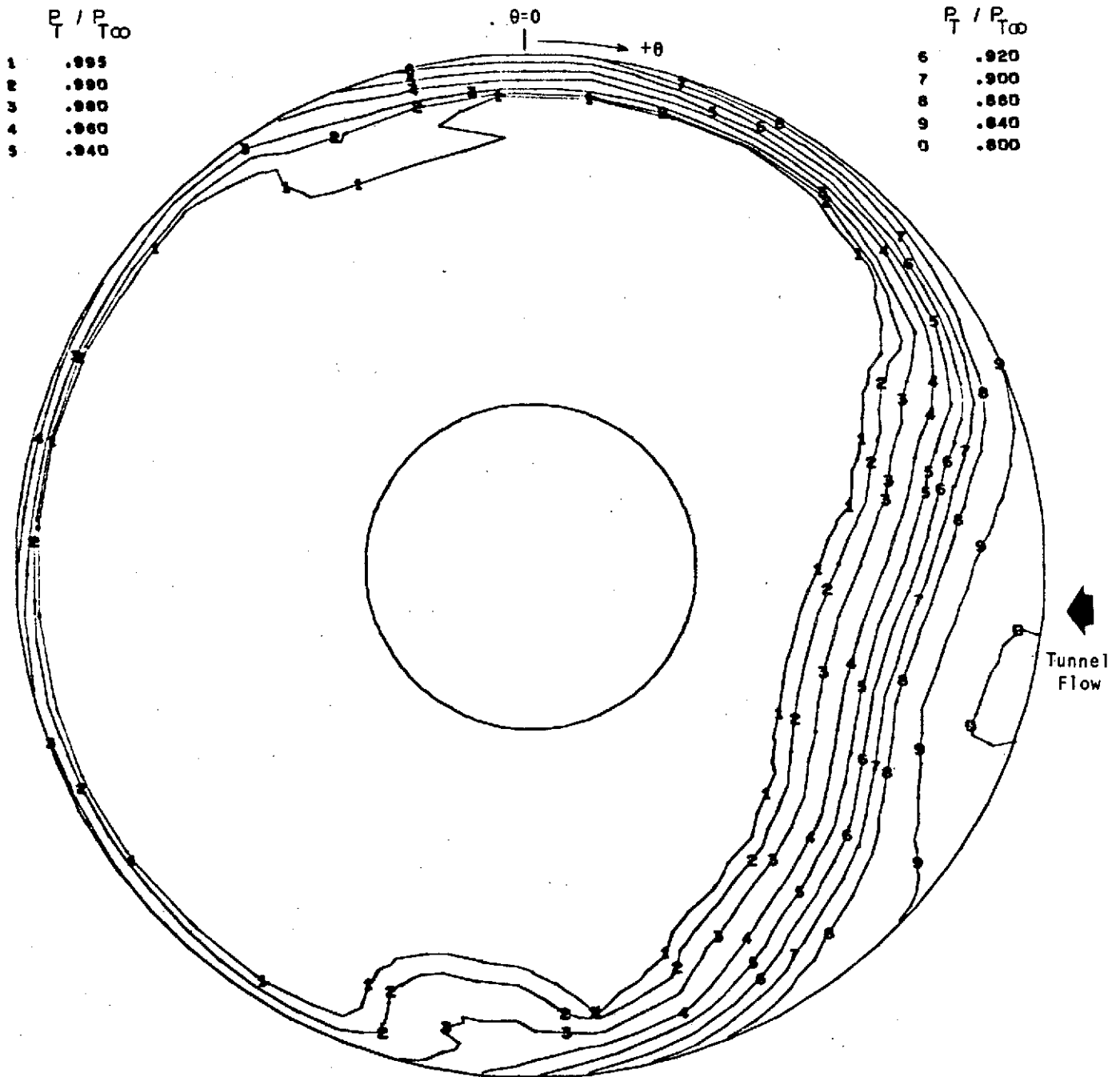
TEST NO. 2390
 RUN NO. 45
 COND. NO. 4.0000

TEST DATE 12/12/73
 RECOVERY .9944
 $w_a \sqrt{\rho_{t2}} / \delta_{t2}$ 468.904 LB/SEC

CALC. DATE 01/16/74
 PRI RECOVERY .9995
 FAN RECOVERY .9919

FIGURE 21 CONFIGURATION 1 ENGINE FACE PRESSURE
 RECOVERY MAP (180 Knots @ $\alpha = 17.5^\circ$)

727 REFAN, SIDE INLET MODEL TEST
 VT= 20 KTS , CONFIGURATION NO. 1 , 90 DEG. X-WIND



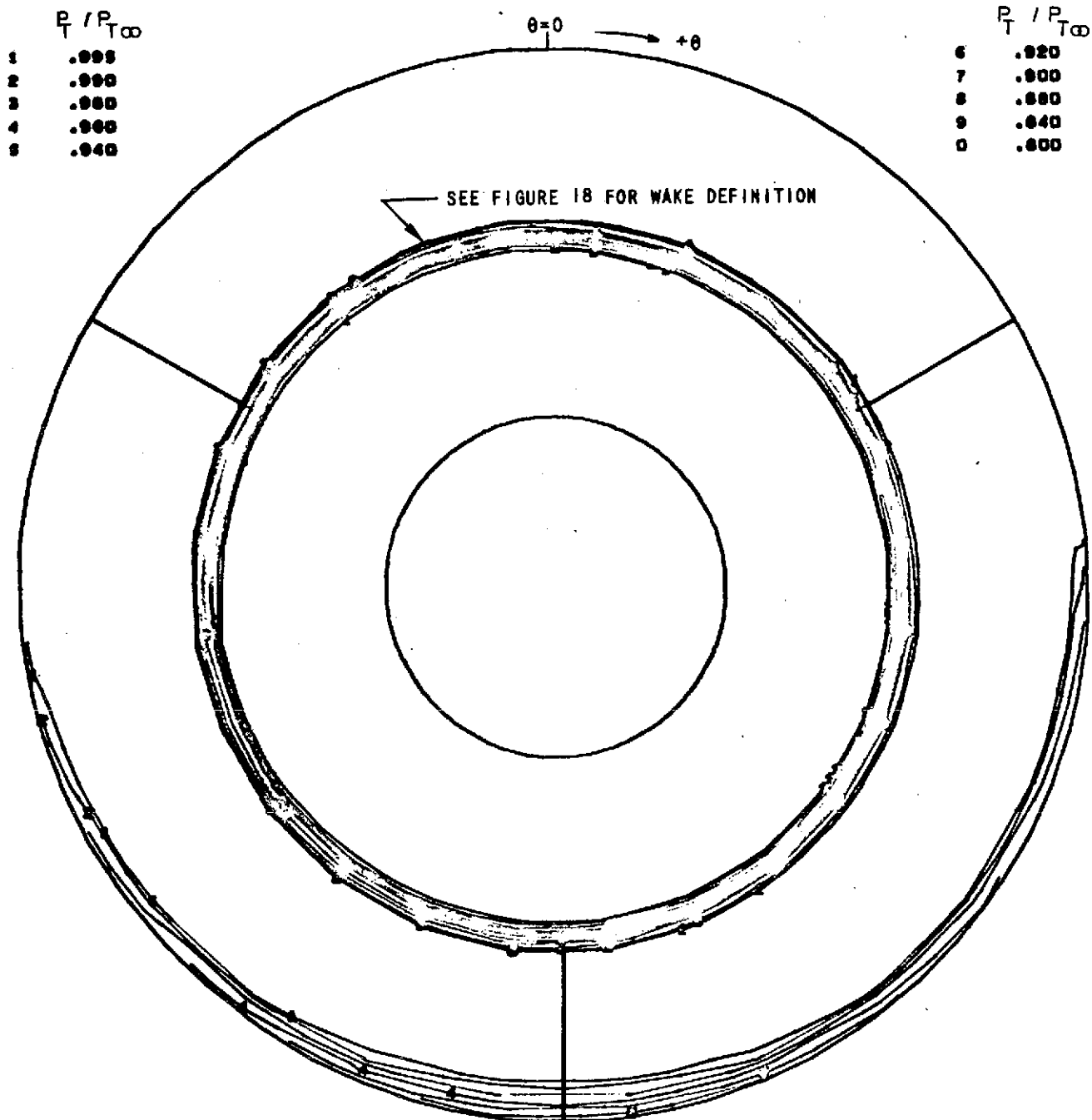
TEST NO. 2390
 RUN NO. 3
 COND. NO. 3.0000

TEST DATE 11/15/73
 RECOVERY .9745
 $W_a \sqrt{g} \delta t_2 / \delta t_2$ 485.492 LB/SEC

CALC. DATE 12/06/73
 PRI RECOVERY .9990
 FAN RECOVERY .9623

FIGURE 22 CONFIGURATION 1 ENGINE FACE PRESSURE
 RECOVERY MAP (20 Knots Cross Wind)

F27 REFAN, SIDE INLET MODEL TEST
 CONFIG. 2, ALPHA = 17.5 DEG. FWD. VELOCITY
 TUNNEL VELOCITY = 180 KNOTS



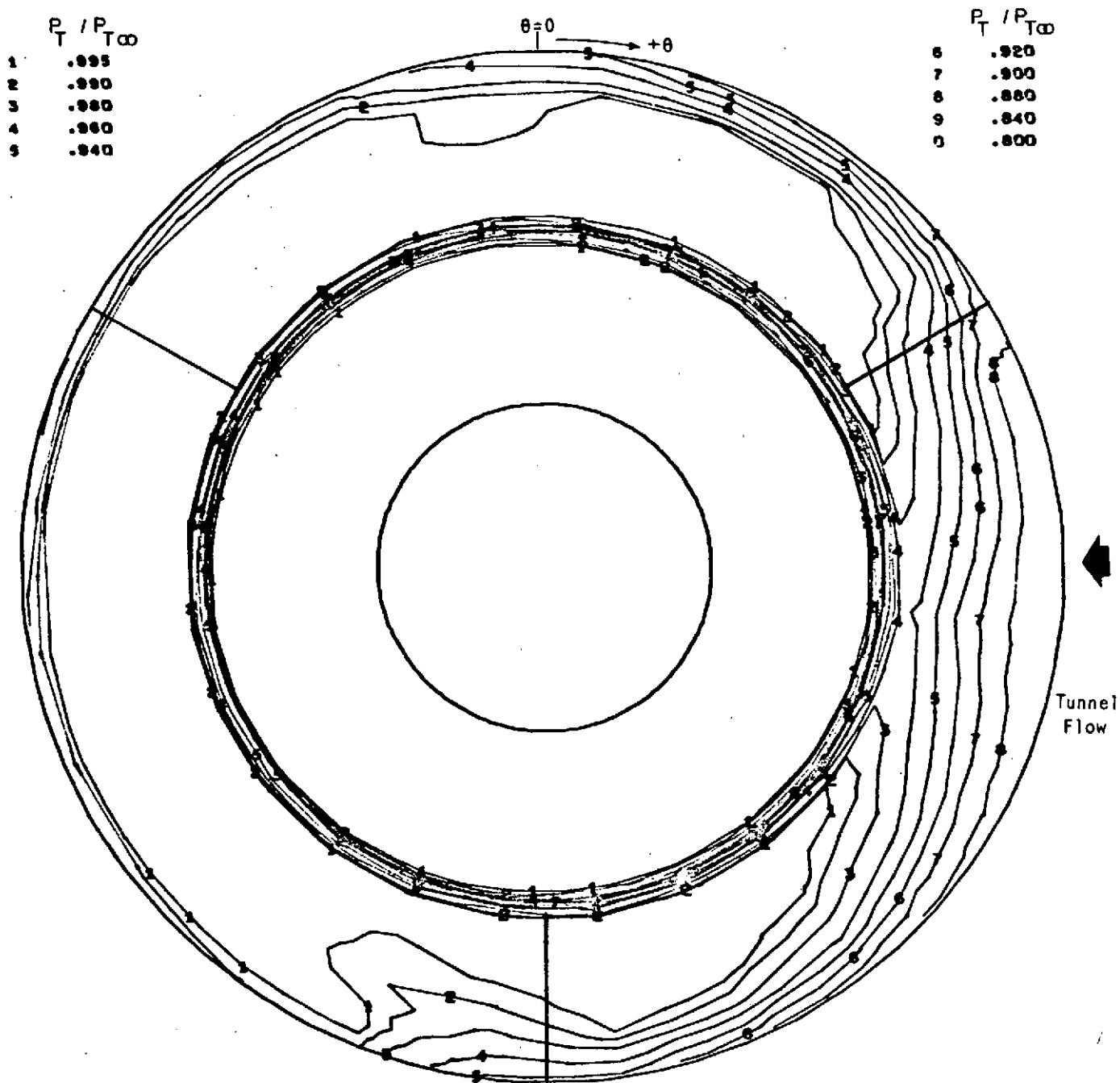
TEST NO. 2390
 RUN NO. 35
 COND. NO. 3.0000

TEST DATE 12/ 5/73
 RECOVERY .9917
 $W_a \sqrt{\theta_{t2} / \delta_{t2}}$ 468.276 LB/SEC

CALC. DATE 01/09/74
 PRI RECOVERY .9992
 FAN RECOVERY .9879

FIGURE 23 CONFIGURATION 2 ENGINE FACE PRESSURE
 RECOVERY MAP (180 Knots @ $\alpha = 17.5^\circ$)

727 REFAN, SIDE INLET MODEL TEST
 VT = 20 KNOTS, CONFIG. 2 , 90 DEG. CROSSWIND



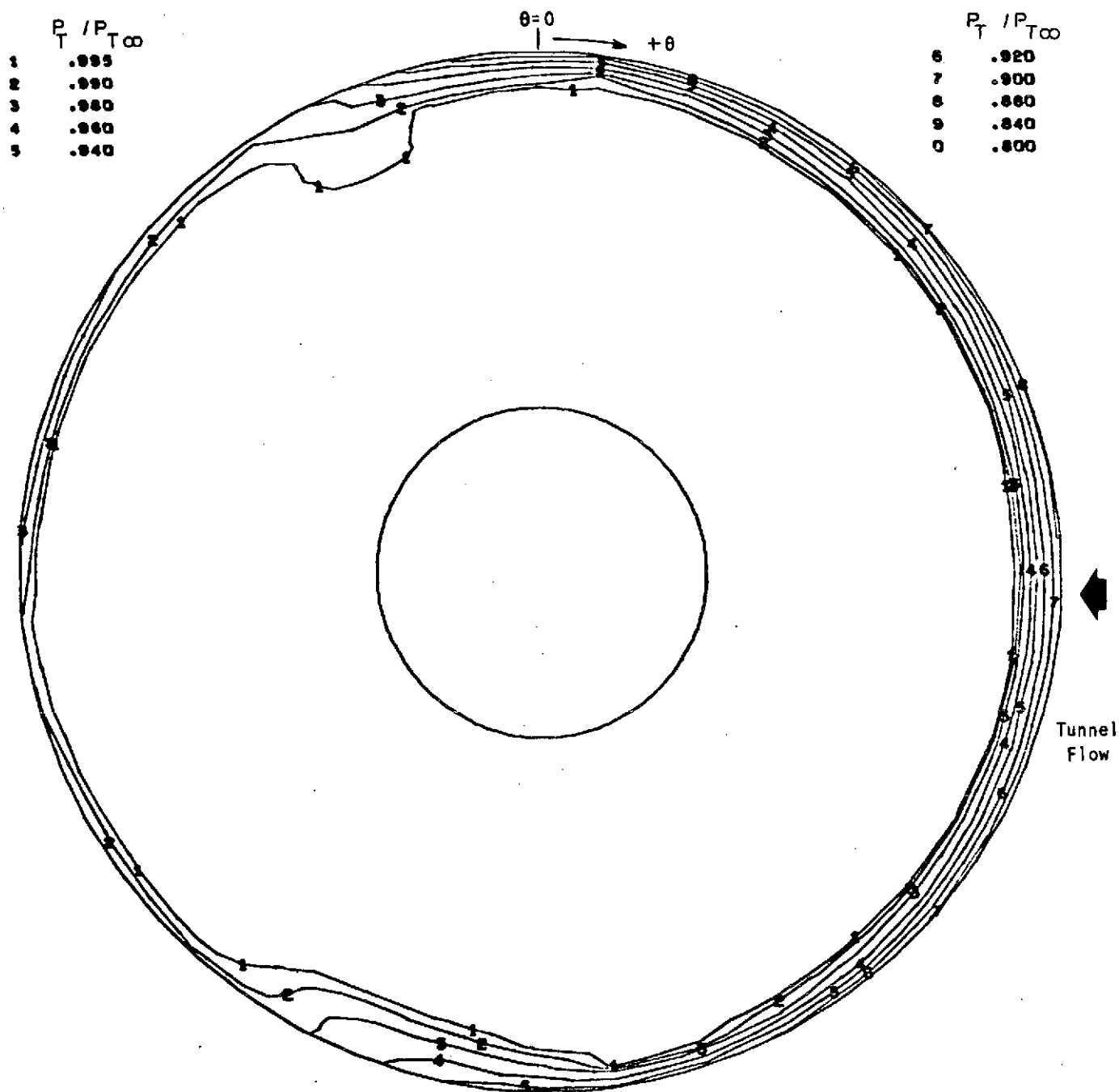
TEST NO. 2390
 RUN NO. 15
 COND. NO. 3.0000

TEST DATE 11/29/73
 RECOVERY .9800
 $W_a \sqrt{\theta t_2 / \delta t_2}$ 472.263 LB/SEC

CALC. DATE 12/13/73
 PRI RECOVERY .9997
 FAN RECOVERY .9701

FIGURE 24 CONFIGURATION 2 ENGINE FACE PRESSURE
 RECOVERY MAP (20 Knots Cross-Wind)

727 REFAN, SIDE INLET MODEL TEST
 VT = 30 KNOTS, CONFIGURATION 1L, 30 PERCENT LIP, 90 DEG. X-WIND



TEST NO. 2390
 RUN NO. 8
 COND. NO. 3.0000

TEST DATE 11/16/73
 RECOVERY .9917
 $w\sqrt{g_2/\delta t_2}$ 480.784 LB/SEC

CALC. DATE 12/06/73
 PRI RECOVERY .9995
 FAN RECOVERY .9878

FIGURE 25 CONFIGURATION 1L ENGINE FACE PRESSURE
 RECOVERY MAP (30 Knots Cross-wind)

727 JT8D-100 SIDE INLET

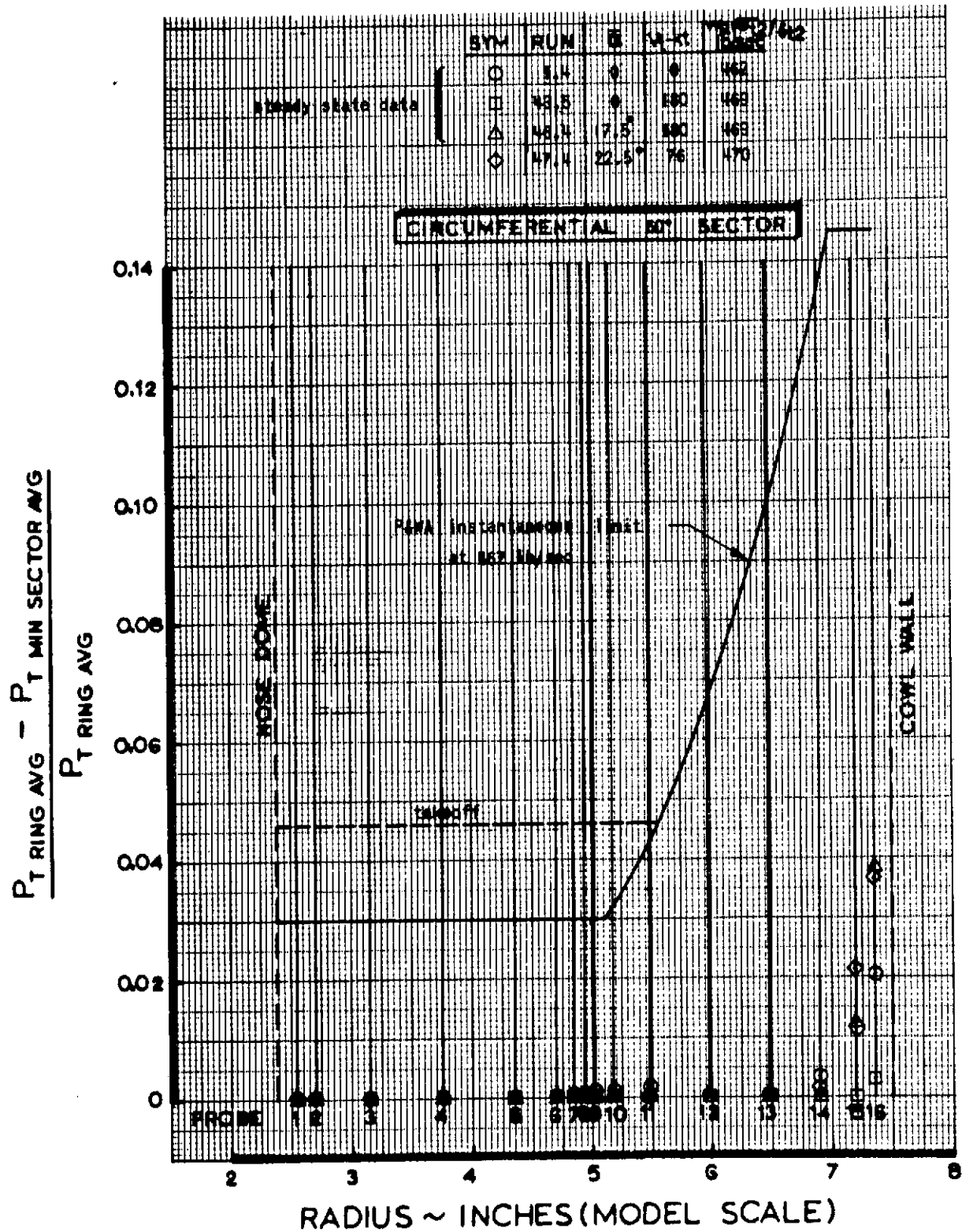


FIGURE 26 CONFIGURATION 1 CIRCUMFERENTIAL PRESSURE DISTORTION 60° SECTOR (Static, Fwd Speed and Angle-of-Attack Conditions)

727 JT8D-100 SIDE INLET

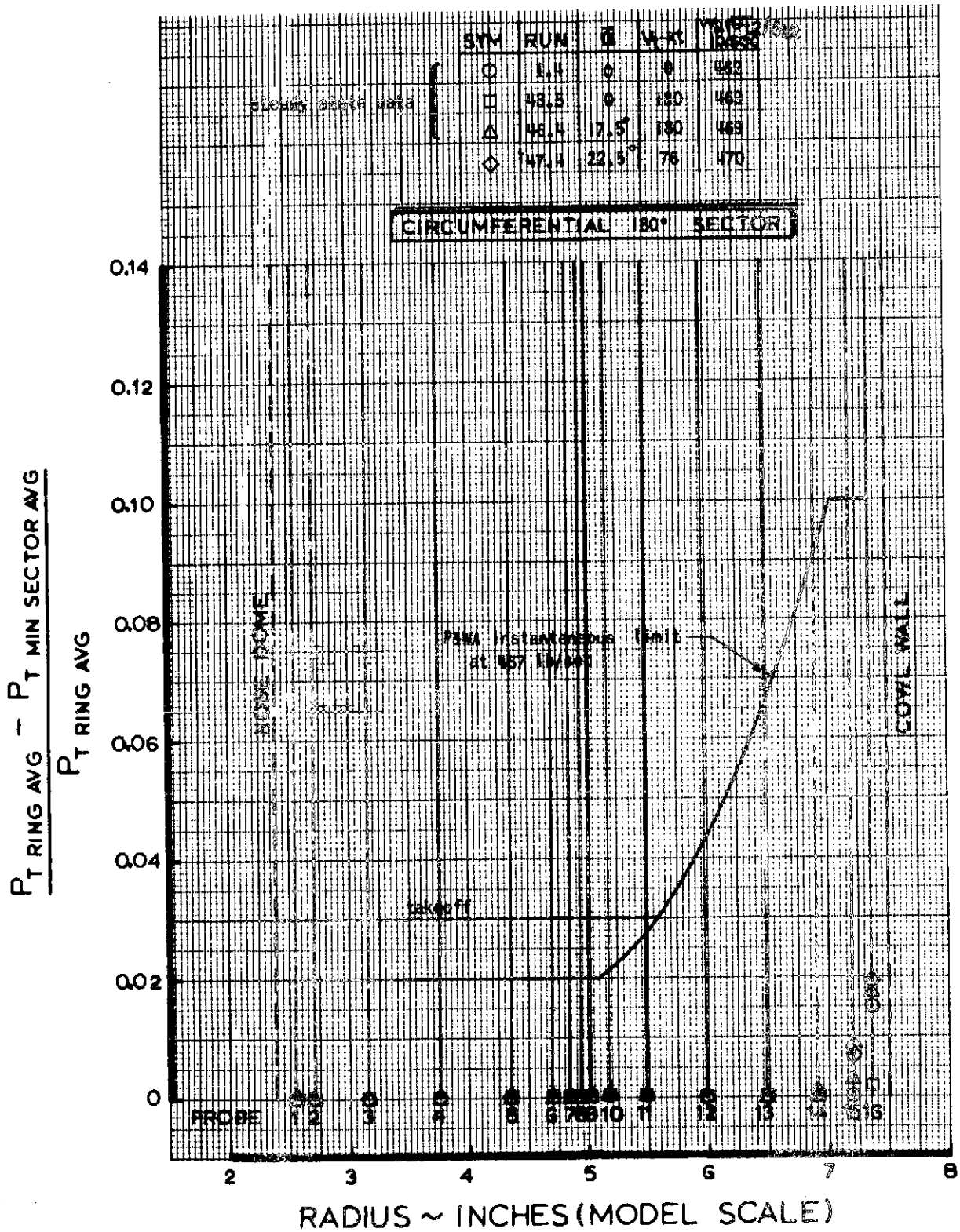


FIGURE 27 CONFIGURATION 1 CIRCUMFERENTIAL PRESSURE
DISTORTION 180° SECTOR (Static, Fwd Speed
and Angle-of-Attack Conditions)

727 JT8D 100 SIDE INLET

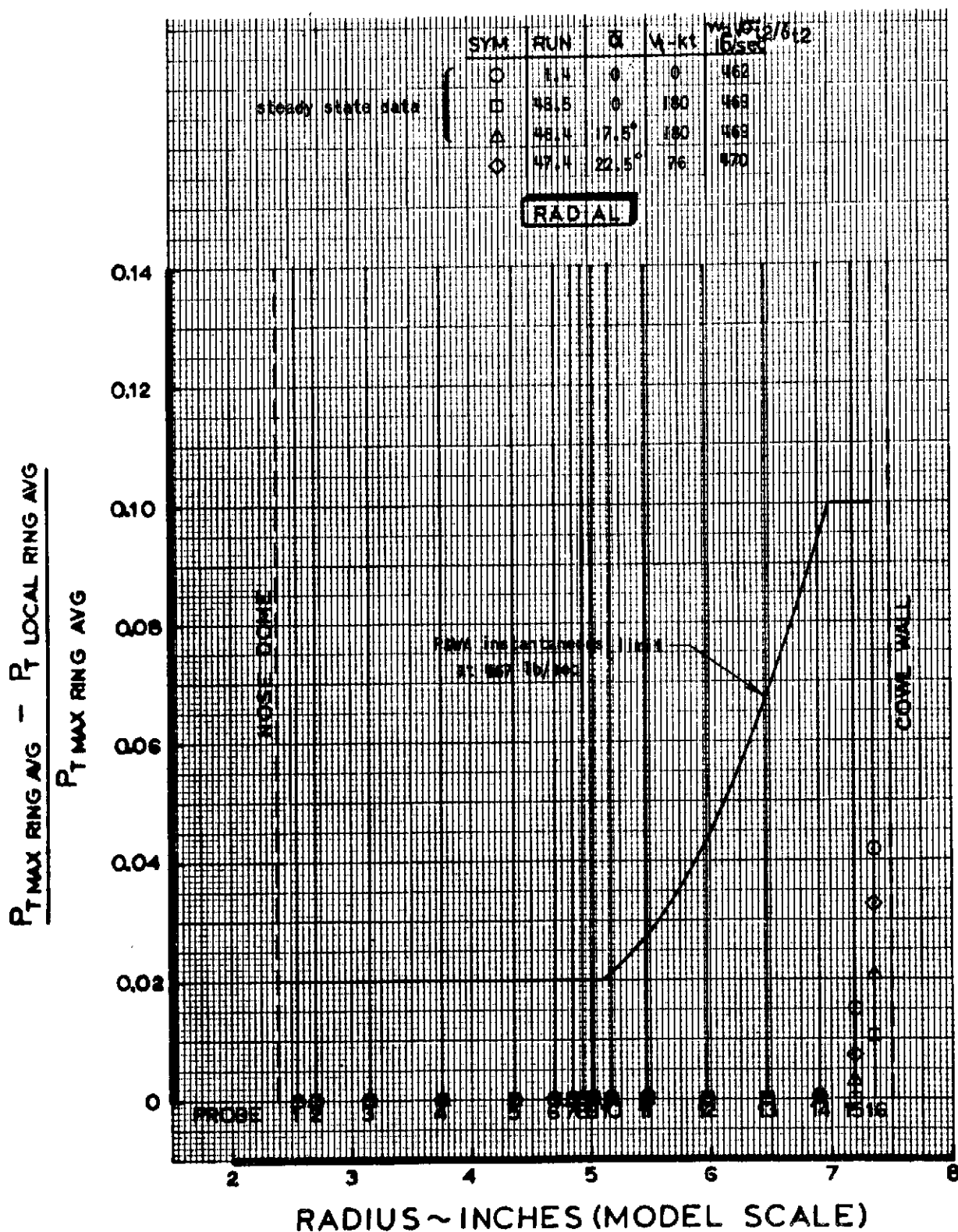


FIGURE 28 CONFIGURATION 1 RADIAL PRESSURE DISTORTION
(Static, Fwd Speed and Angle-of-Attack Conditions)

727 JTBD-100 SIDE INLET

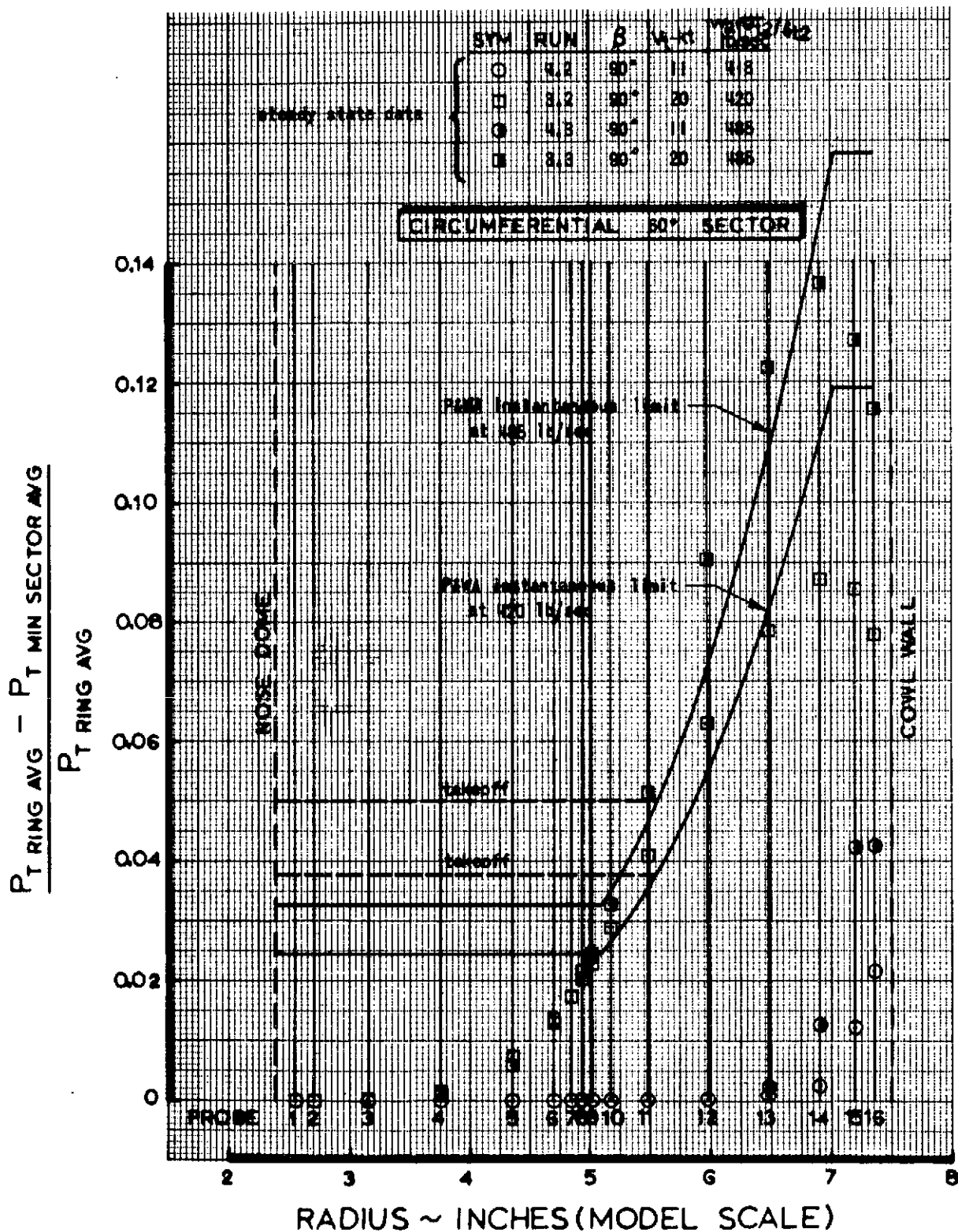


FIGURE 29 CONFIGURATION 1 CIRCUMFERENTIAL PRESSURE DISTORTION 60° SECTOR (Cross-Wind Conditions)

727 JT8D-100 SIDE INLET

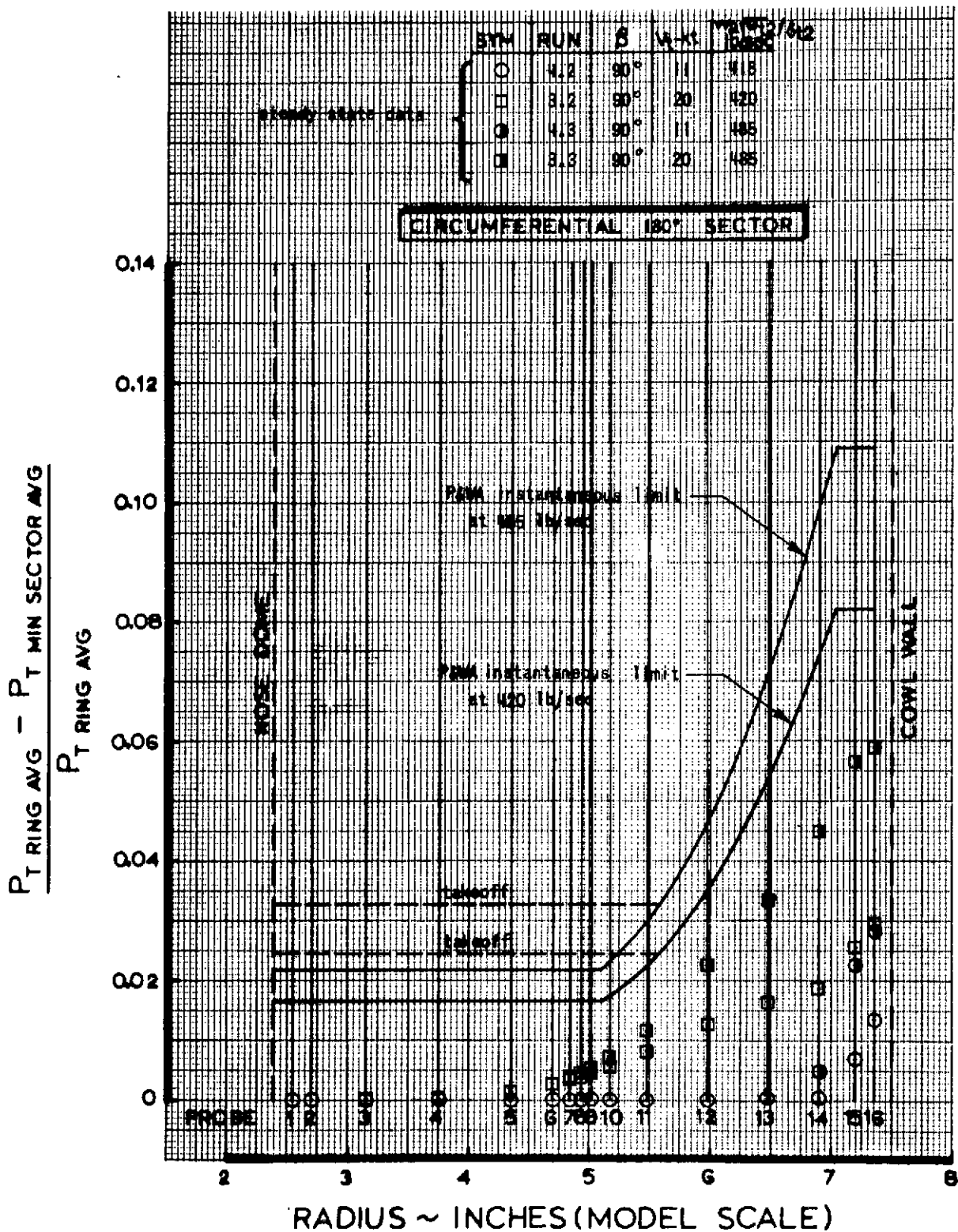


FIGURE 30 CONFIGURATION 1 CIRCUMFERENTIAL PRESSURE DISTORTION 180° SECTOR (Cross-Wind Conditions)

727 JTBD 100 SIDE INLET

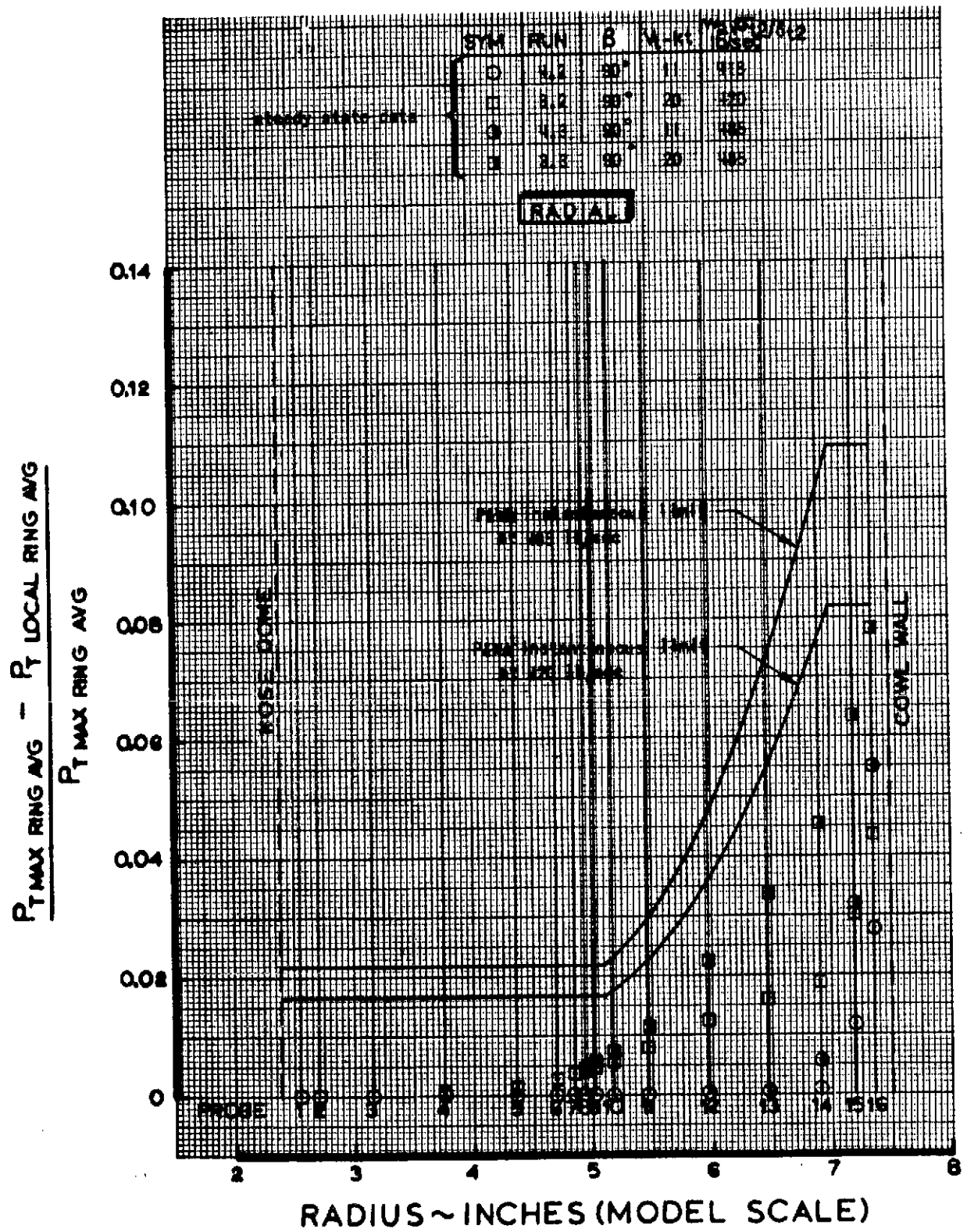


FIGURE 31 CONFIGURATION 1 RADIAL PRESSURE DISTORTION (Cross-Wind Conditions)

727 JT8D-100 SIDE INLET

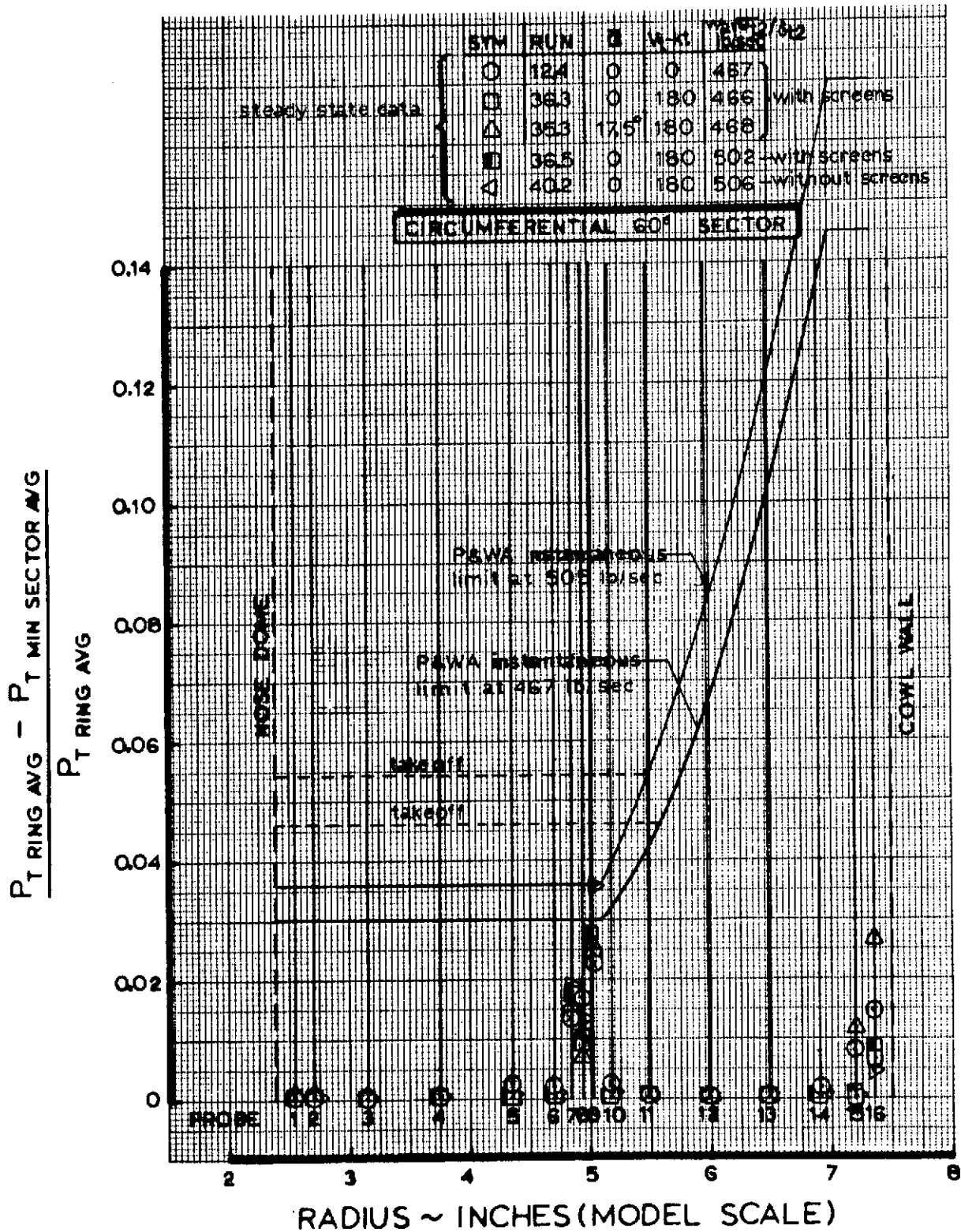


FIGURE 32 CONFIGURATION 2 CIRCUMFERENTIAL PRESSURE DISTORTION 60° SECTOR (Static, Fwd Speed and Angle-of-Attack Conditions)

727 JT8D-100 SIDE INLET

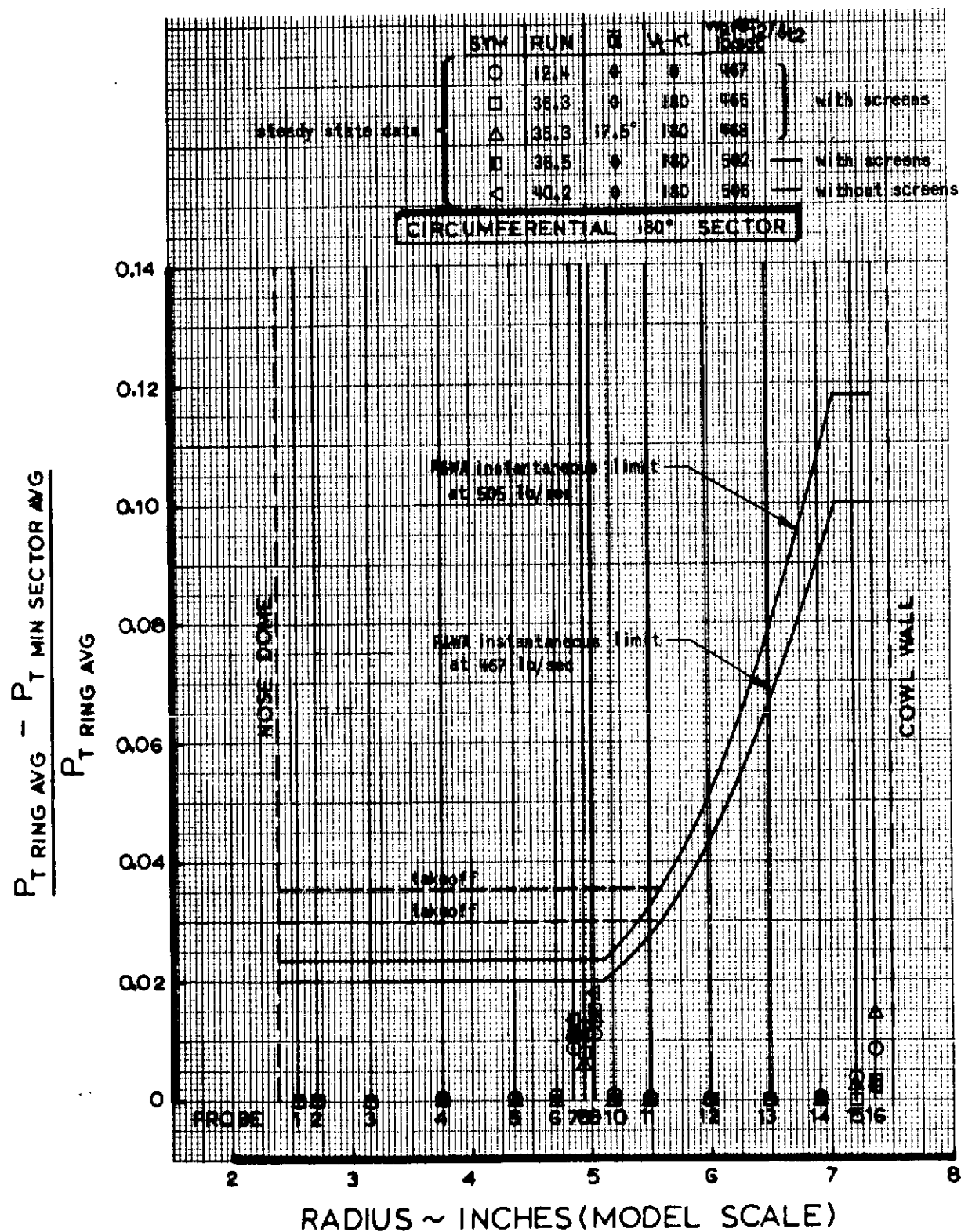


FIGURE 33 CONFIGURATION 2 CIRCUMFERENTIAL PRESSURE DISTORTION 180° SECTOR (Static, Fwd Speed and Angle-of-Attack Conditions)

727 JT8D 100 SIDE INLET

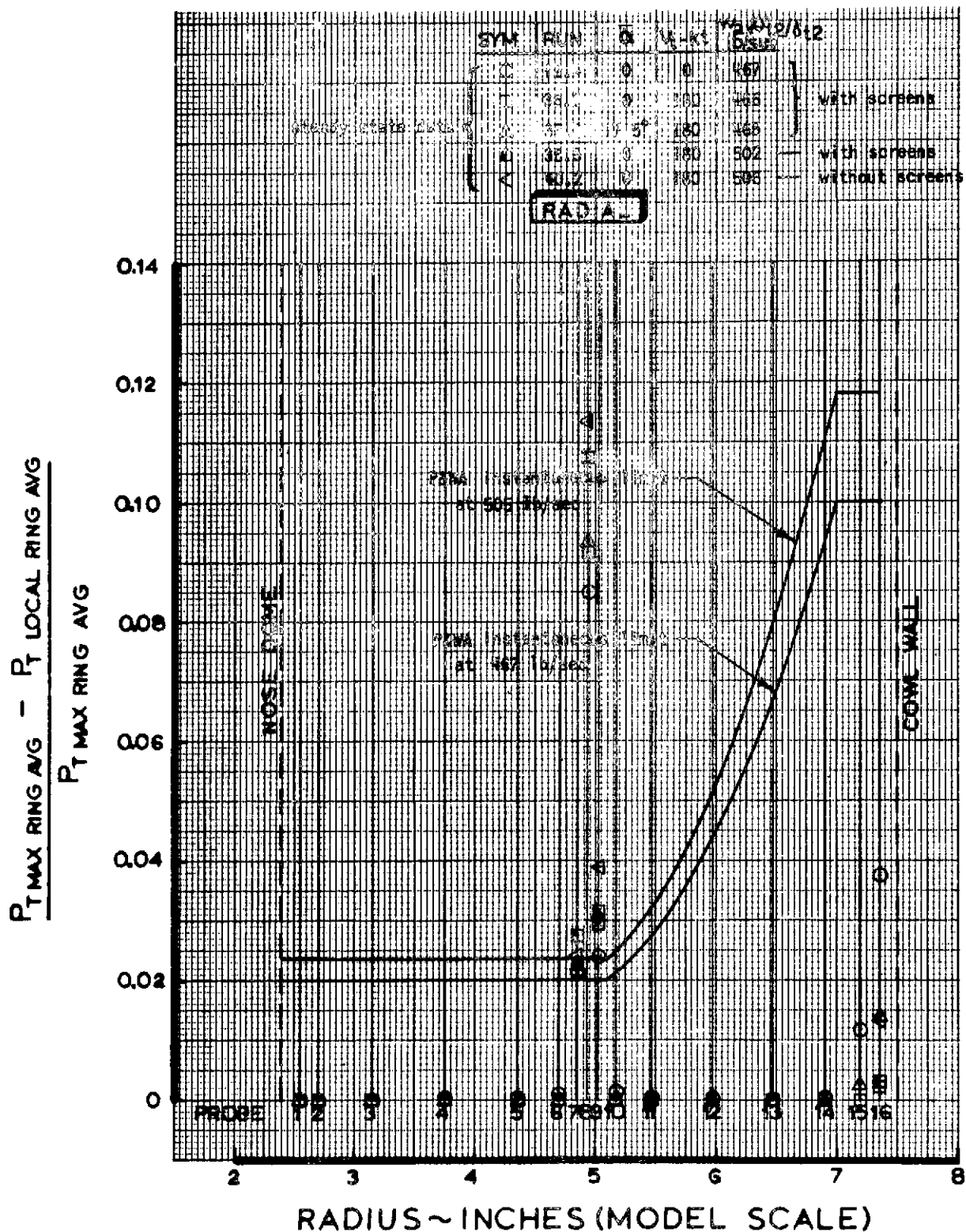


FIGURE 34 CONFIGURATION 2 RADIAL PRESSURE DISTORTION
(Static, Fwd Speed and Angle-of-Attack Conditions)

727 JY8D-100 SIDE INLET

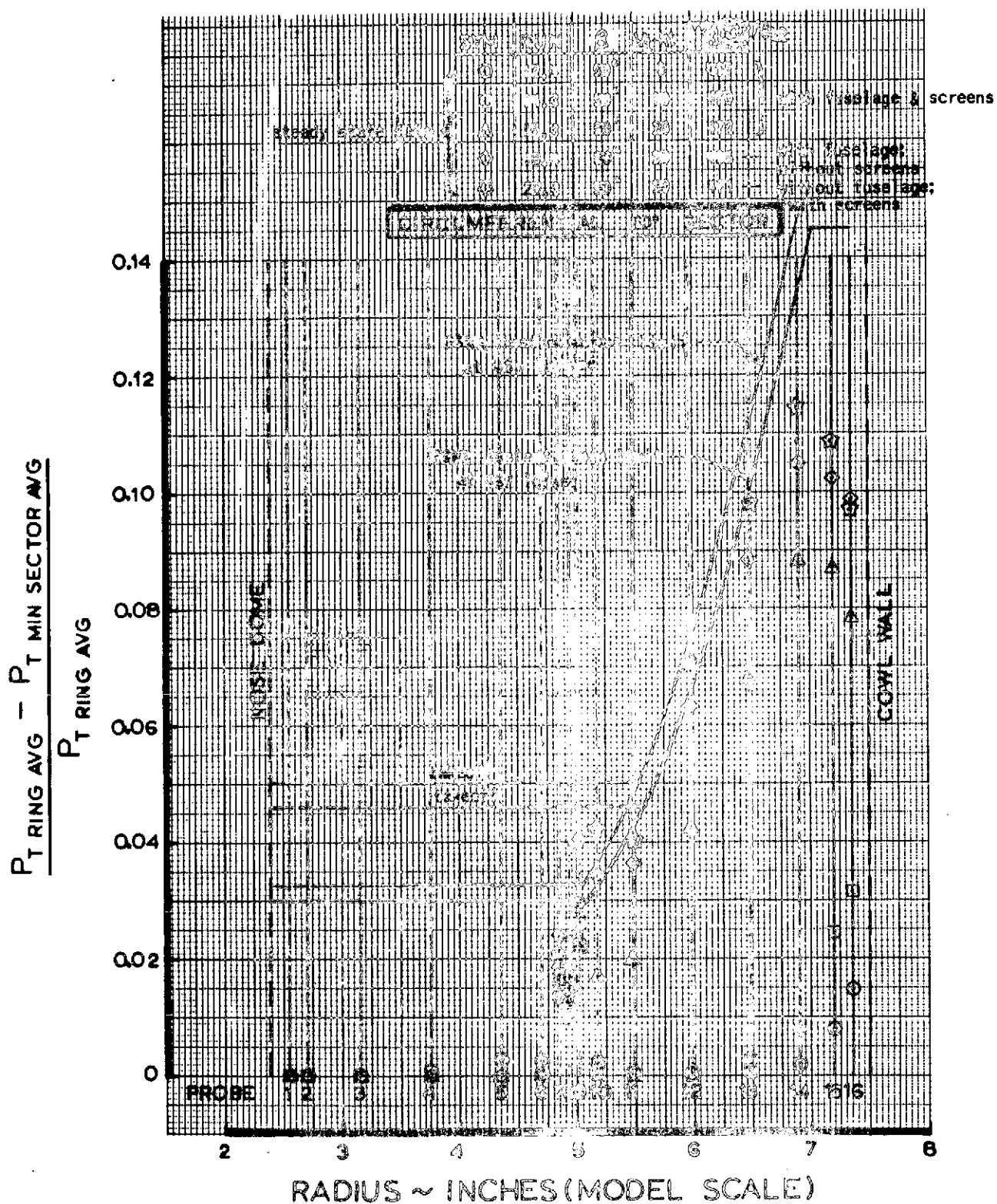


FIGURE 35 CONFIGURATION 2 CIRCUMFERENTIAL PRESSURE DISTORTION 60° SECTOR (Static and Cross-Wind Conditions)

727 JT8D-100 SIDE INLET

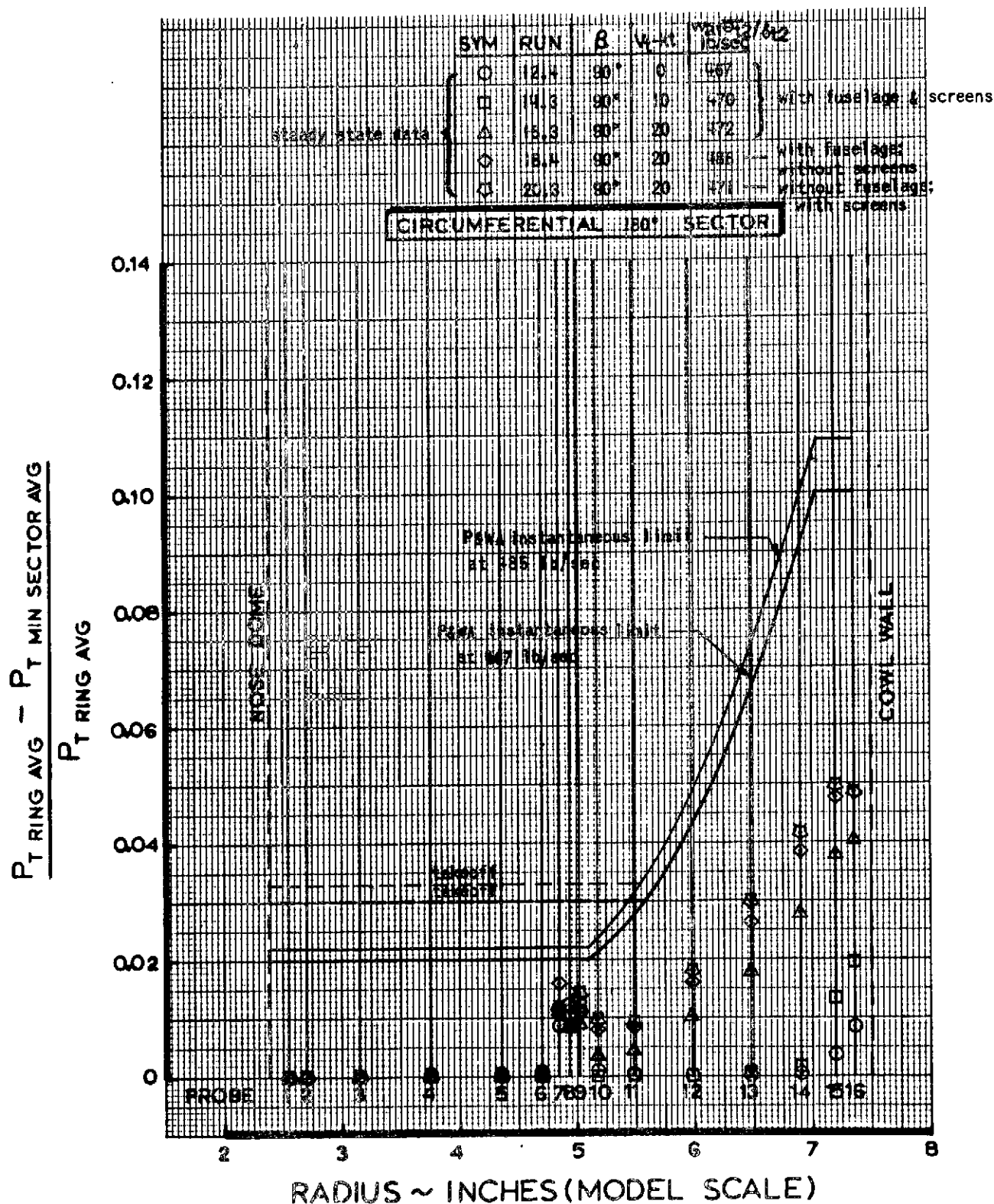


FIGURE 36 CONFIGURATION 2 CIRCUMFERENTIAL PRESSURE DISTORTION 180° SECTOR (Static and Cross-Wind Conditions)

727 JT8D 100 SIDE INLET

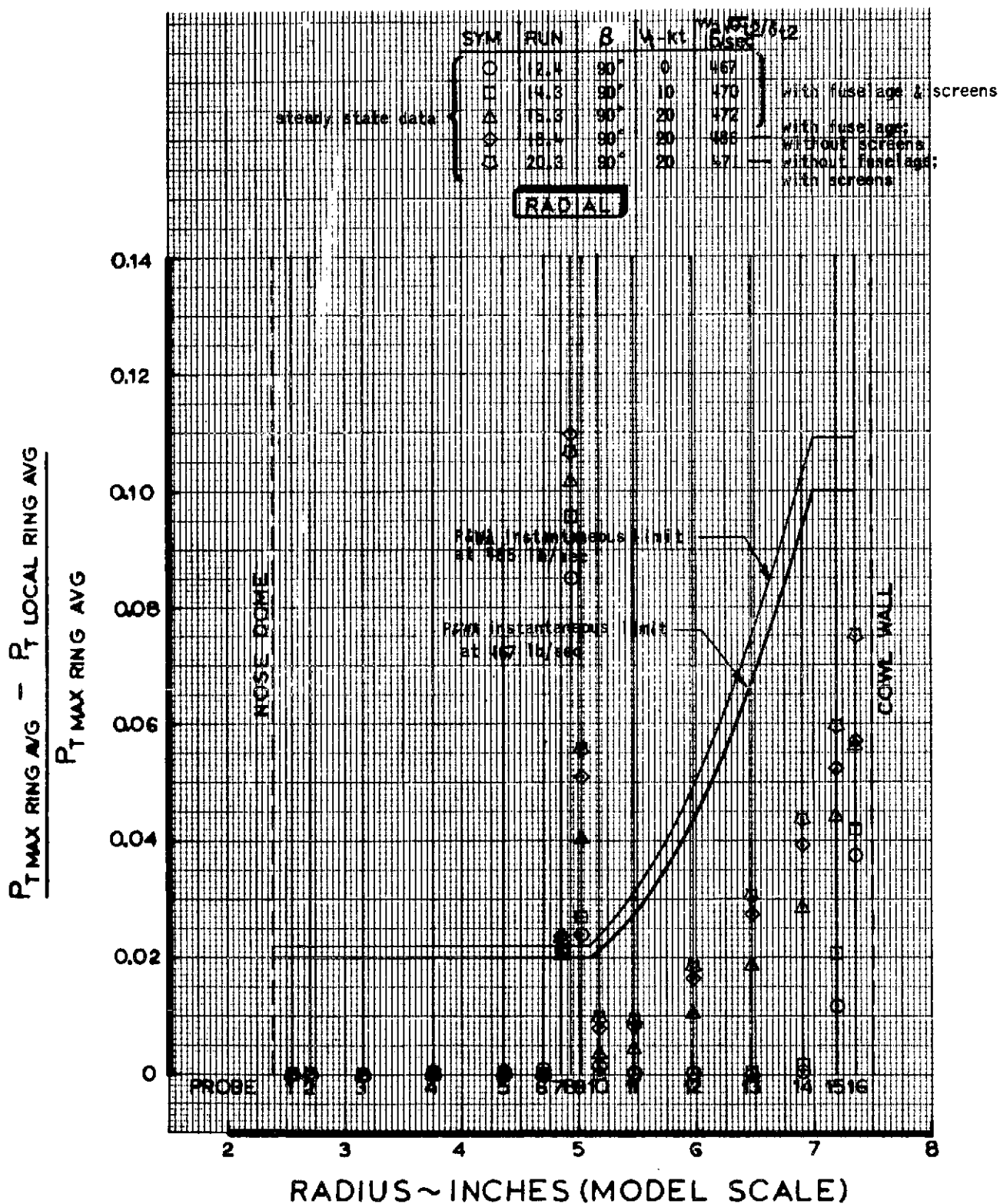


FIGURE 37 CONFIGURATION 2 RADIAL PRESSURE DISTORTION
(Static and Cross-Wind Conditions)

727 JT8D-100 SIDE INLET

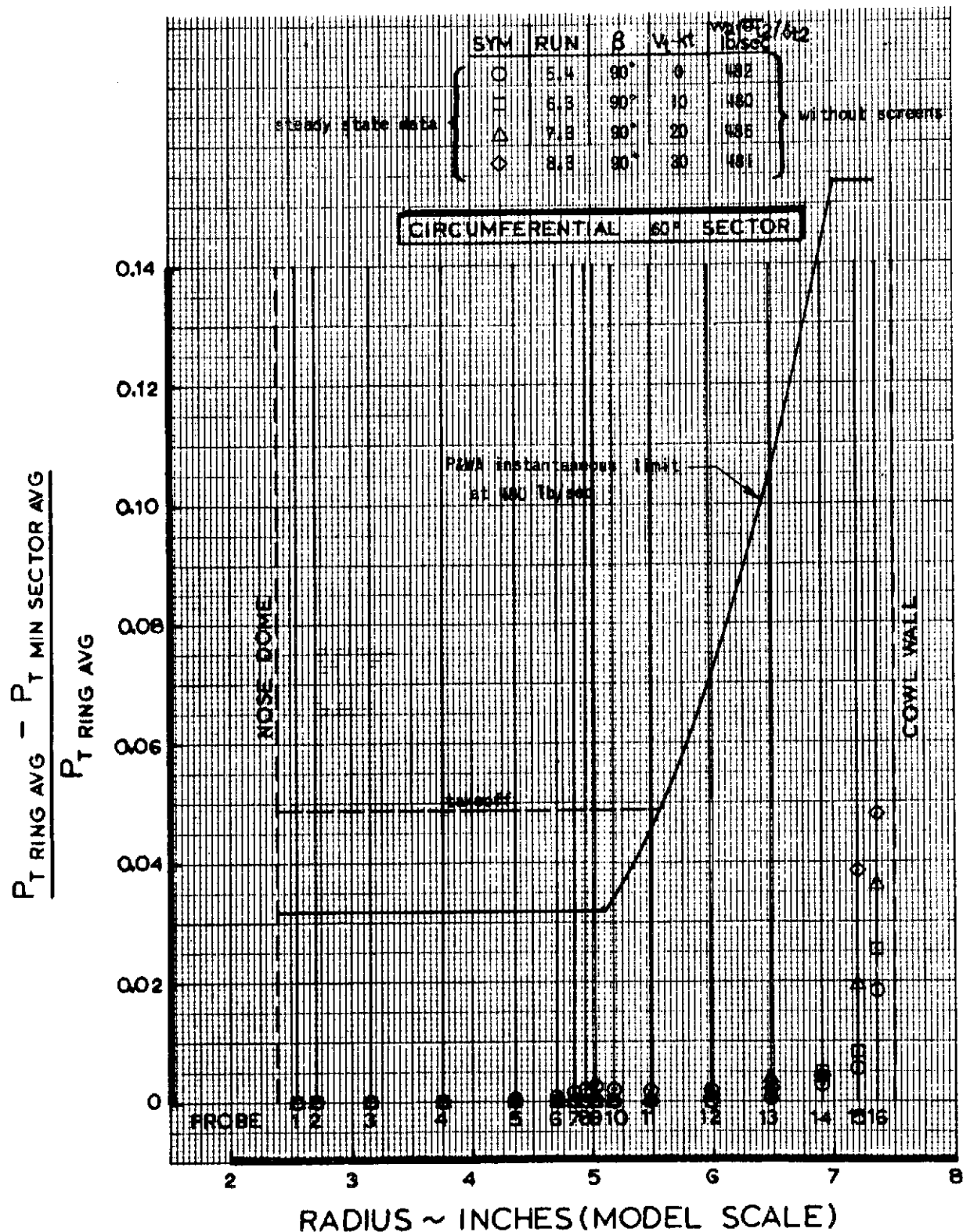


FIGURE 38 CONFIGURATION 1L CIRCUMFERENTIAL PRESSURE DISTORTION 60° SECTOR (Static and Cross-Wind Conditions)

727 JT8D-100 SIDE INLET

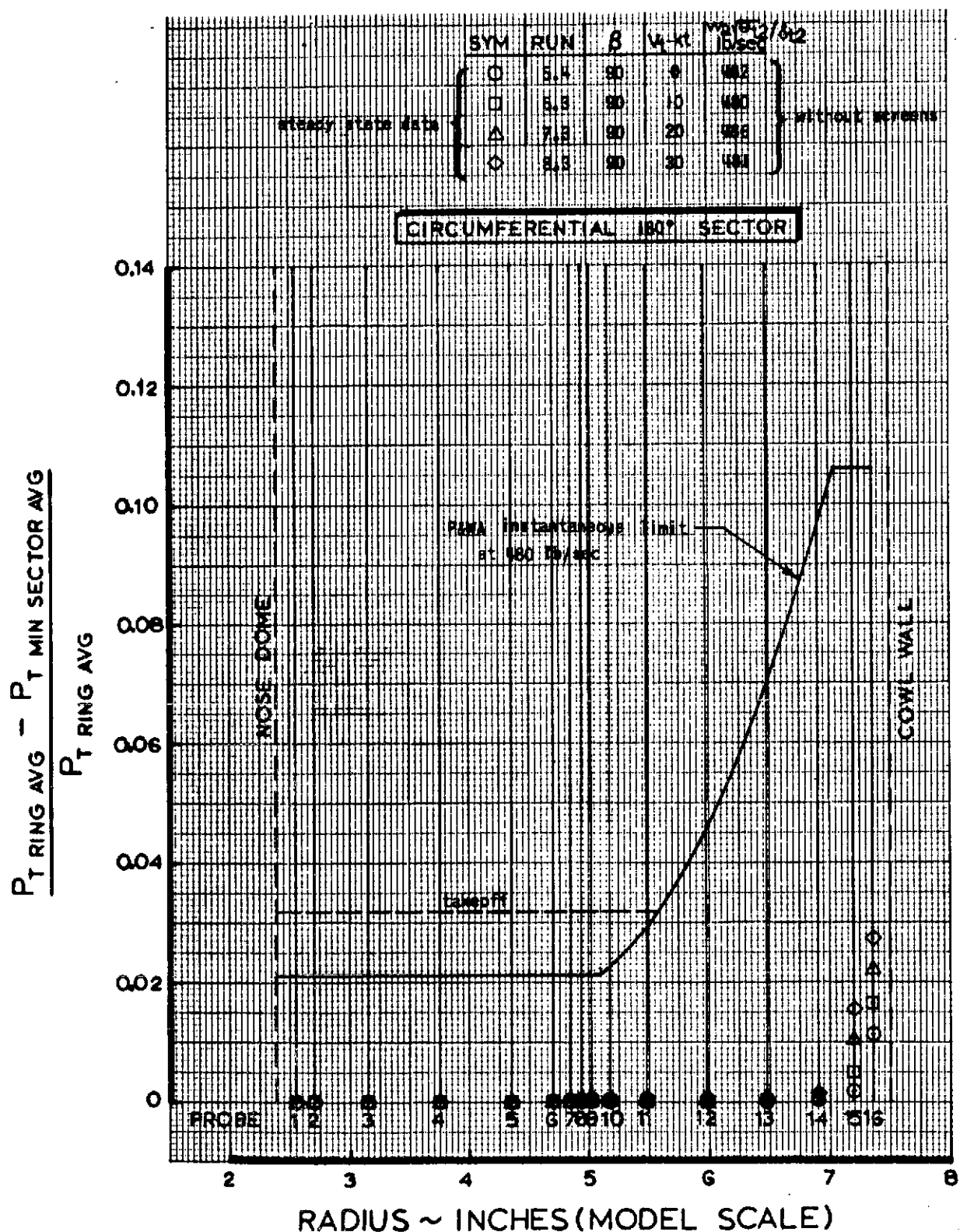


FIGURE 39 CONFIGURATION 1L CIRCUMFERENTIAL PRESSURE DISTORTION 180° SECTOR (Static and Cross-Wind Conditions)

727 JT8D 100 SIDE INLET

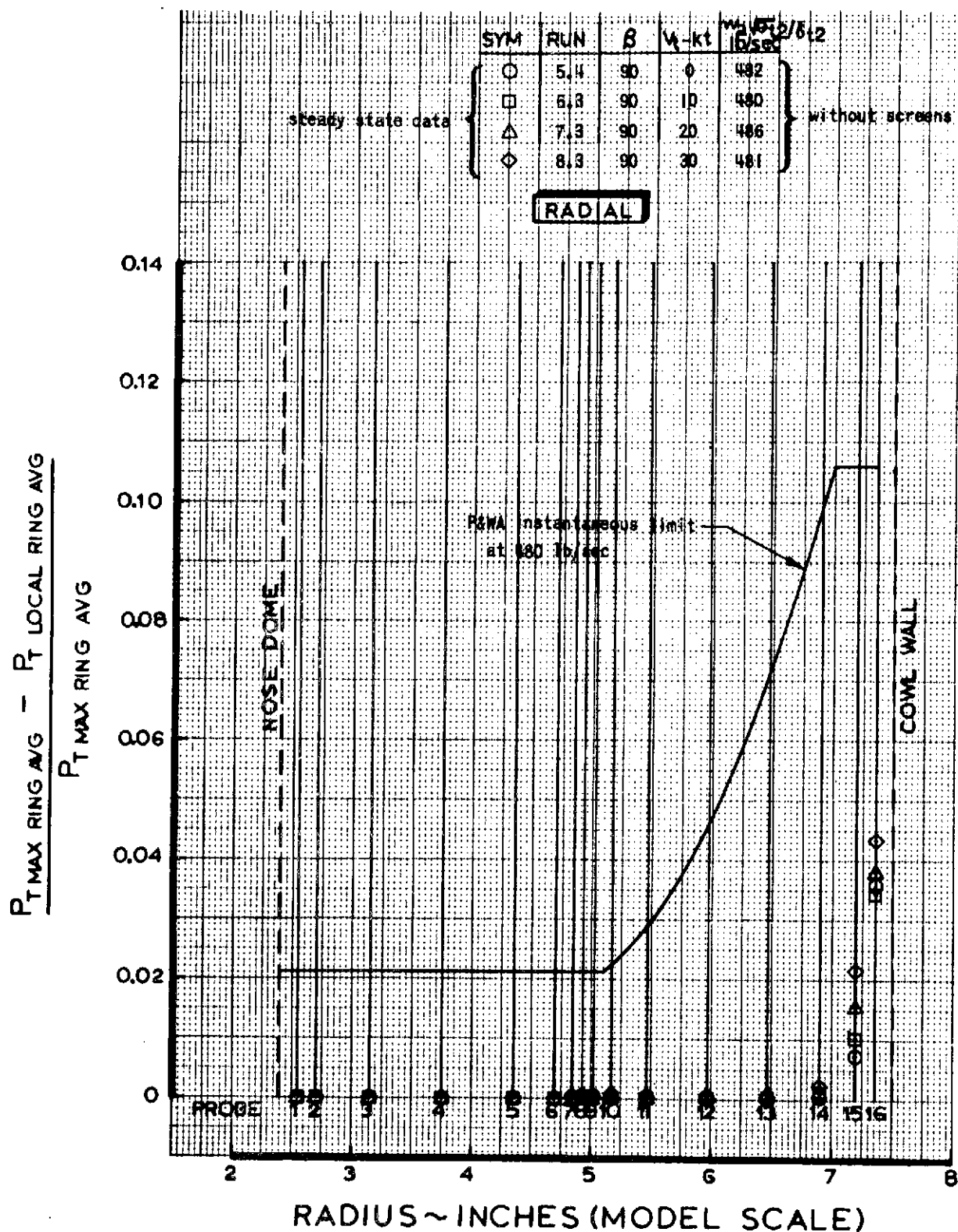
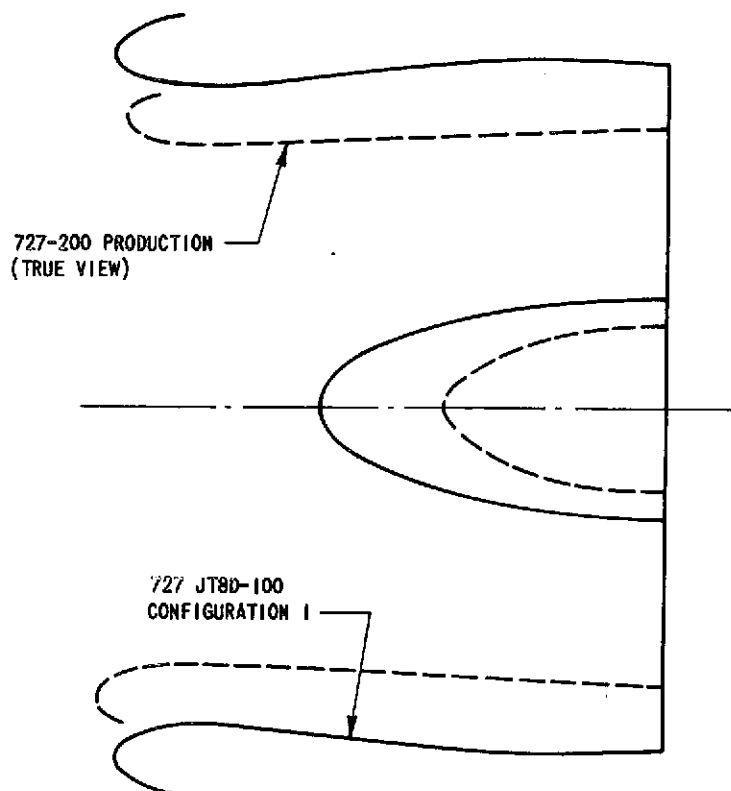


FIGURE 40 CONFIGURATION 1L RADIAL PRESSURE DISTORTION
(Static and Cross-Wind Conditions)



* The production inlet is identical on all JT8D series engines.

	727-200 JT8D-100	727-200 * (PRODUCTION) JT8D-15
Max. cruise corrected airflow, $W_a \sqrt{\theta_{t2}} / \delta_{t2} \sim \text{lb/sec}$	480	326
$M_{\infty} = 0.8$, 30,000 feet, std. day		
Highlight diameter ~ inches	52.21	42.305
Highlight area ~ sq. in.	2141.07	1405.64
Lip loading, $W_a \sqrt{\theta_{t2}} / \delta_{t2} A_{HI} \sim \text{lb/sec-ft}^2$	32.28	33.40
Highlight Mach number	0.420	0.438
Throat diameter ~ inches	46.70	37.84
Throat area ~ sq. in.	1712.87	1124.59
Throat Mach number	0.572	0.604
Contraction ratio (highlight area / throat area)	1.25	1.25
Lip contour	2.5:1 super ellipse	2.111:1 ellipse
Distance between inlet & and fuselage ~ inches	44.5 (approximate)	39.01
Engine face diameter ~ inches	50.10	40.50
Nose dome diameter ~ inches	16.00	12.030
Engine face area ~ sq. in.	1770.29	1174.59
Engine face area / throat area	1.034	1.044
Engine face Mach number	0.543	0.563
Nose dome length ~ inches	25.20	15.038
Degrees of cant	0.0	4.0
Length / engine face diameter	0.8	1.0

FIGURE 41 DESIGN COMPARISON OF 727 PRODUCTION AND JT8D-100 SIDE INLETS

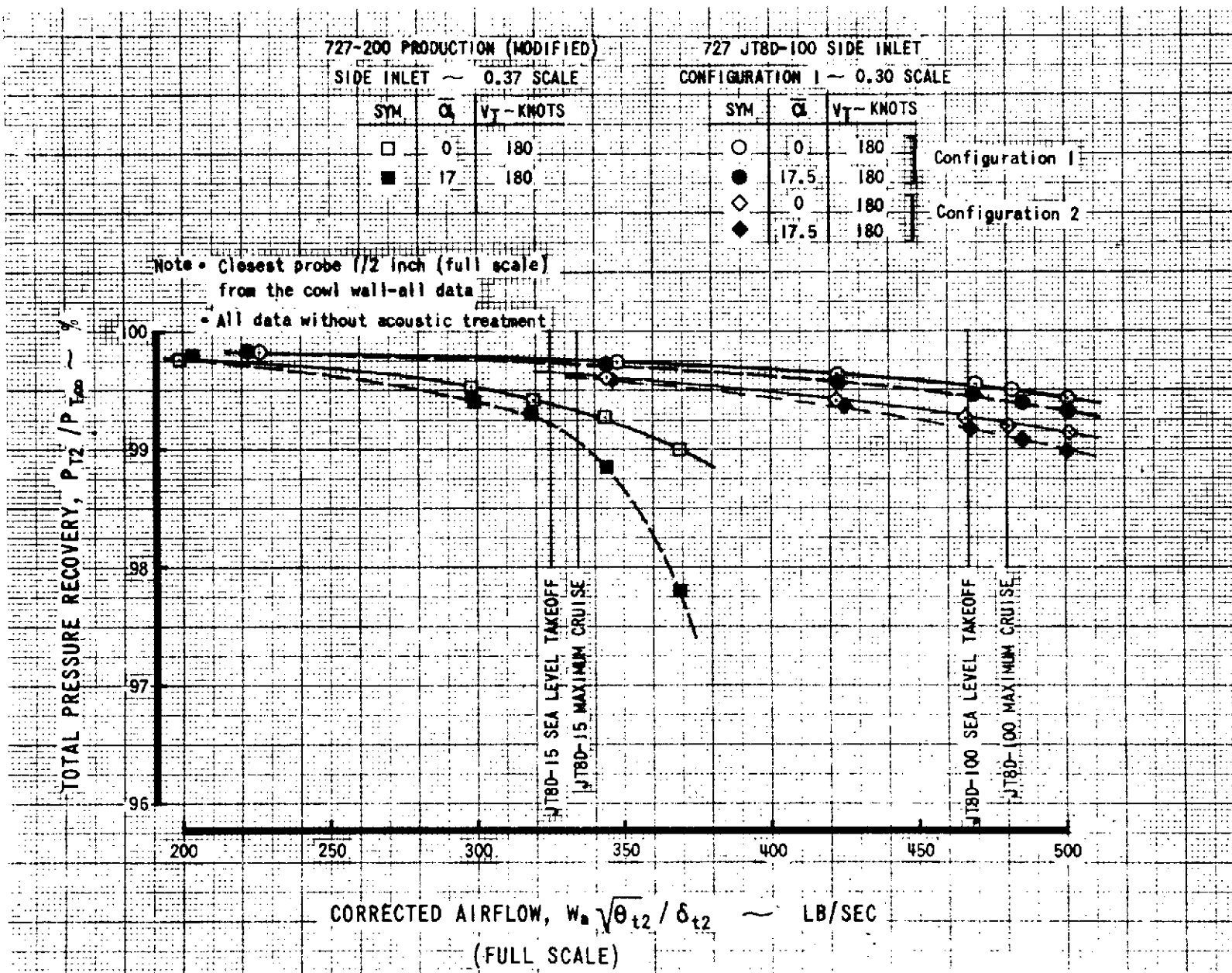


FIGURE 42 PRESSURE RECOVERY COMPARISON 727-200 PRODUCTION (Modified) AND JT8D-100 SIDE INLETS

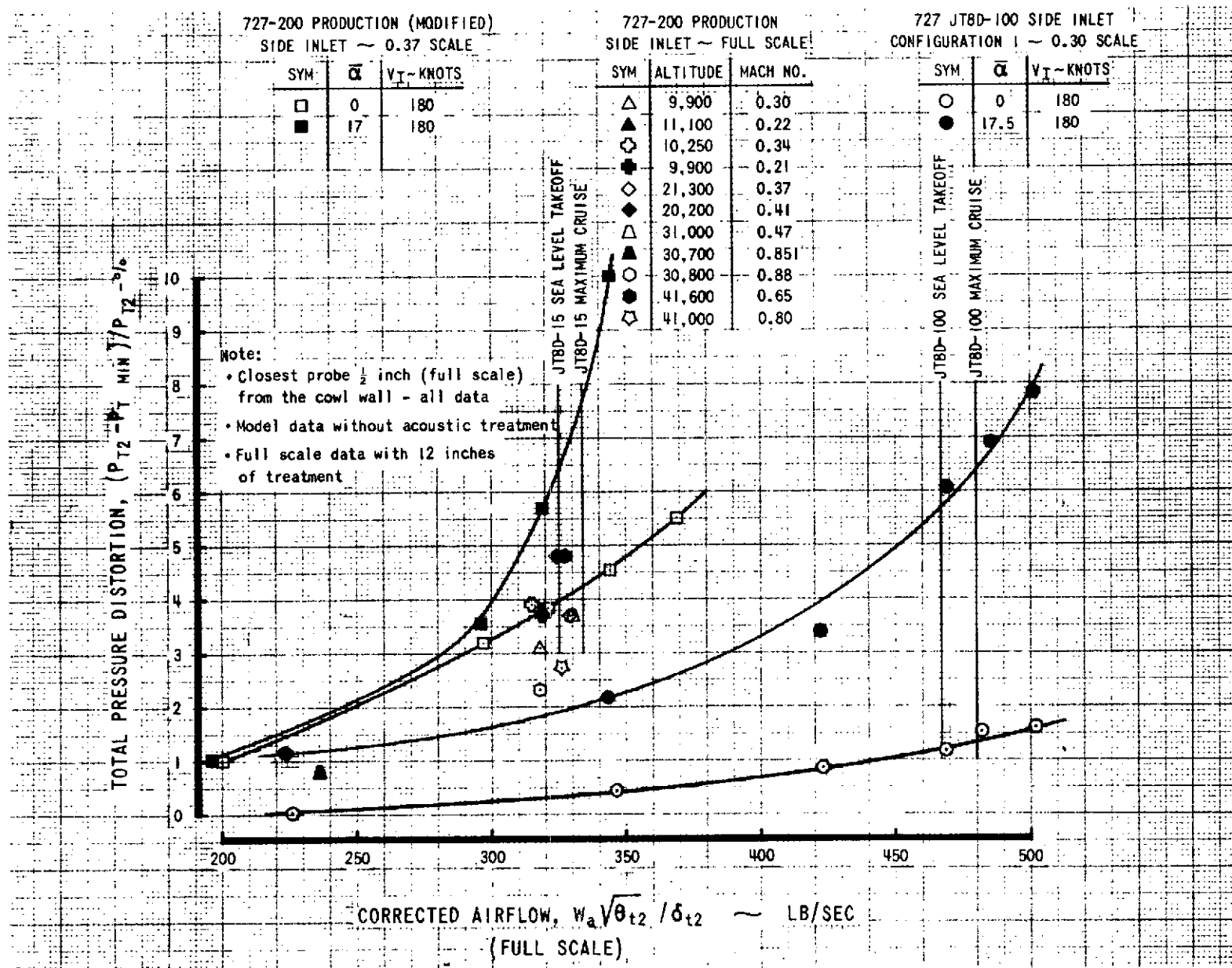


FIGURE 43 TOTAL PRESSURE DISTORTION COMPARISON 727-200 PRODUCTION AND JT8D-100 SIDE INLETS

APPENDIX A SYMBOLS

APPENDIX A

SYMBOLS

a	Half the major axis of an ellipse
A_{HI}	Highlight area (or Hilite)
A_{TH}	Throat area
BBL	Body Buttock Line
BWL	Body Water Line
b	Half the minor axis of an ellipse
D_2	Engine face diameter
K_t	Knots
L	Inlet length
L.E.	Leading edge
MCR	Maximum Cruise
MCT	Maximum Continuous Thrust
M_∞	Free stream Mach number
M_{TH}	Throat Mach number (one dimensional)
M_2	Engine face Mach number (one dimensional)
$P_{T\infty}$	Freestream (tunnel) total pressure
P_T	Engine face total pressure measurement
$P_{T \text{ Min}}$	Minimum engine face total pressure measured
$P_{T \text{ Max}}$	Maximum engine face total pressure measured
P_{T2}	Area average (see Section 3.4) of engine face total pressure measurements
$P_{T2}/P_{T\infty}$	Total pressure recovery
$P_T \text{ Ring Avg.}$	} Average engine face total pressure at a given radius
$P_T \text{ Local Ring Avg}$	

Preceding page blank

P_T Max Ring Avg	The maximum average engine face total pressure computed at the given radii (Maximum P_T Ring Avg)
P_T Min Sector Avg	Average engine face total pressure at a given radius in the minimum total pressure sector (for 60 or 180 degree sectors)
R	Inlet Radius
T_{T2}	Total temperature at engine face (average)
V_t	Tunnel velocity
V_∞	Freestream velocity
T.E.	Trailing edge
W_a	Actual airflow
$W_a \sqrt{\theta_{t2}} / \delta_{t2}$	Engine face corrected airflow
X	Inlet centerline distance, or coordinate in ellipse equation
Y	Coordinate in ellipse equation
α	Inlet angle-of-attack (inflow angle) relative to engine and inlet
β	Inlet yaw angle relative to inlet
θ	Angular position around engine face
θ_{t2}	$T_{T2}/518.7$ when T_{T2} is in degrees Rankine
δ_{t2}	$P_{T2}/14.69$ when P_{T2} is in pounds per square inch

APPENDIX B
INLET COORDINATES

APPENDIX B-INLET COORDINATES

ALL MODELS AXIALLY SYMMETRIC
ALL DIMENSIONS INCHES FULL SCALE

COWL CONFIGURATIONS 1, 2, and 2R
(CONFIGURATION 1L from $X_c = 33.2$ to -9)

X_c	R	COMMENT	X_c	R	COMMENT
6.631	31.000	Contour not critical in this region	37.200	23.766	(The lip contour is extremely critical)
14.092	30.945		36.700	23.652	
17.784	30.658		35.700	23.489	
24.476	30.123		34.700	23.394	
27.822	29.745		33.700	23.354	
31.168	29.272	External Cowl	33.200	23.350	- Throat
33.398	28.890		33.000	23.3505	
35.629	28.421		32.000	23.364	
37.302	27.962		31.000	23.398	
38.417	27.553		30.000	23.449	
39.254	27.137	NASA Refan Nacelle Crown Contour - Full 360°	28.000	23.600	Internal Cowl
39.532	26.950		26.000	23.806	
39.755	26.756		24.000	24.046	
39.867	26.631		22.000	24.295	
39.9785	26.469		20.000	24.532	
40.034	26.3579	- Hillite	16.000	24.922	
40.090	26.1061		14.000	25.059	
40.000	25.558		12.000	25.150	
39.900	25.340		10.000	25.190	
39.800	25.182		8.000	25.179	
39.600	24.943	Lip - Super Ellipse $\frac{x}{a}^{2.2} + \frac{y}{b}^{2.2} = 1$	6.000	25.137	
39.400	24.758		4.000	25.090	
39.200	24.606		3.000	25.072	
38.700	24.308		2.000	25.060	
38.200	24.084		1.000	25.052	
37.700	23.907		0.000	25.050	- Eng. Face, slope = 0
			0. to -9	25.050	

NOSE DOME
CONFIGURATIONS 1, 2, and 1L

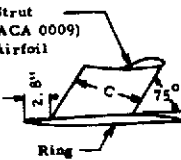
X_c	R	COMMENT
25.200	0.00	- Nose
25.000	1.006	
24.000	2.439	
23.000	3.269	
22.000	3.902	
20.000	4.867	(3.15:1 Ellipse)
18.000	5.599	
16.000	6.181	
12.000	7.035	
8.000	7.586	
4.000	7.898	
2.000	7.975	
0.00	8.000	- Eng. Face, Slope = 0
0. to -9	8.000	

RING-CONFIGURATION 2

STRUTS - CONFIGURATION 2

x/c	y/c	x/c	y/c
.00	.00	.300	.04501
.0125	.0142	.400	.04352
.025	.01961	.500	.03971
.050	.02666	.600	.03423
.075	.03150	.700	.02748
.100	.03512	.800	.01967
.150	.04009	.900	.01086
.200	.04303	.950	.00605
.250	.04456	1.00	.00095

Note: C = 10.3 inches, perpendicular to leading edge
L. E. Radius = .0089XC
Struts @ 120° intervals



NOSE		
X_c	R	Slope
27.179	14.835 (+)	50.1°
27.200	14.770	
27.168	14.709 (-)	39.9°

[L. E. Radius = .090"
With Center @ $X_c = 27.11$,
R = 14.778]

X_c	Inside Radius	Outside Radius
27.179	-	14.835
27.168	14.709	-
27.050	14.646	14.937
26.800	14.579	15.044
26.500	14.547	15.120
26.150	14.536	15.190
25.800	14.547	15.243
25.500	14.569	15.273
25.000	14.614	15.318
24.500	14.658	15.362
24.000	14.703	15.407
23.000	14.792	15.496
22.000	14.881	15.585
18.000	15.237	15.941
16.000	15.415	16.119
14.000	15.593	16.297
12.000	15.738	16.439
10.002	15.858	16.559
8.000	15.944	16.646
6.000	16.025	16.700
5.000	16.076	16.696
4.000	16.140	16.670
3.000	16.222	16.622
2.500	16.271	16.589
2.050	16.319	16.554
1.500	16.385	16.504
1.000	16.4507	16.4507

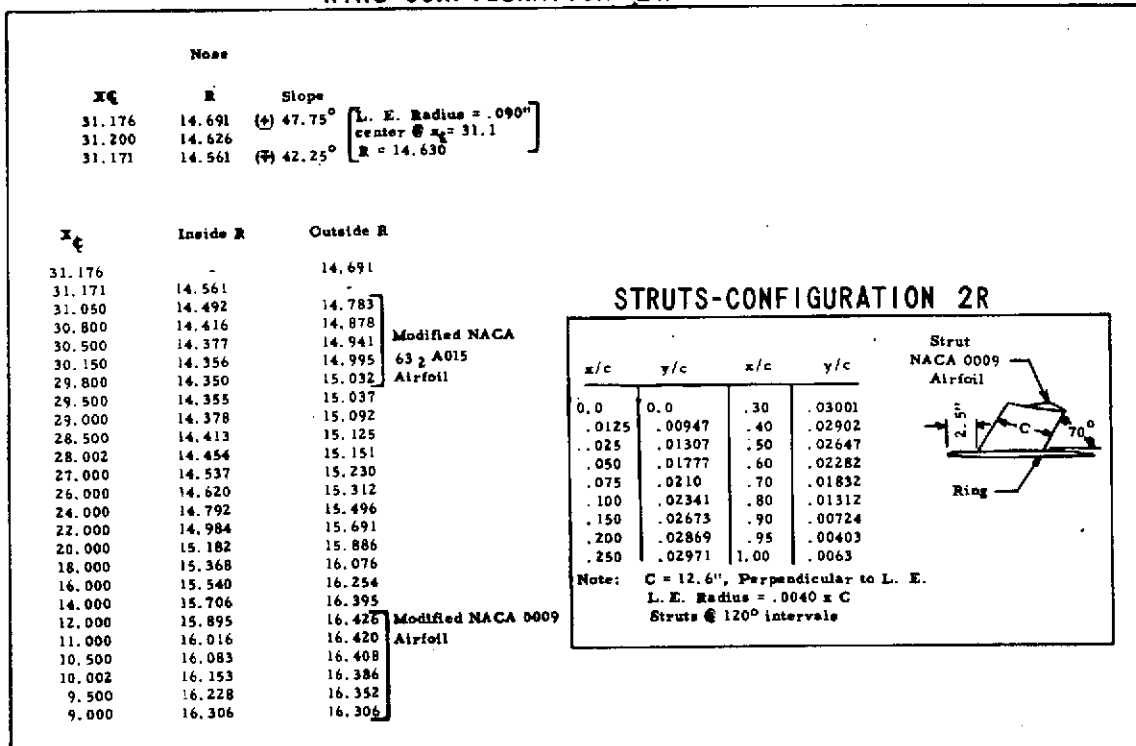
Modified NACA 63₂ A015

Straight

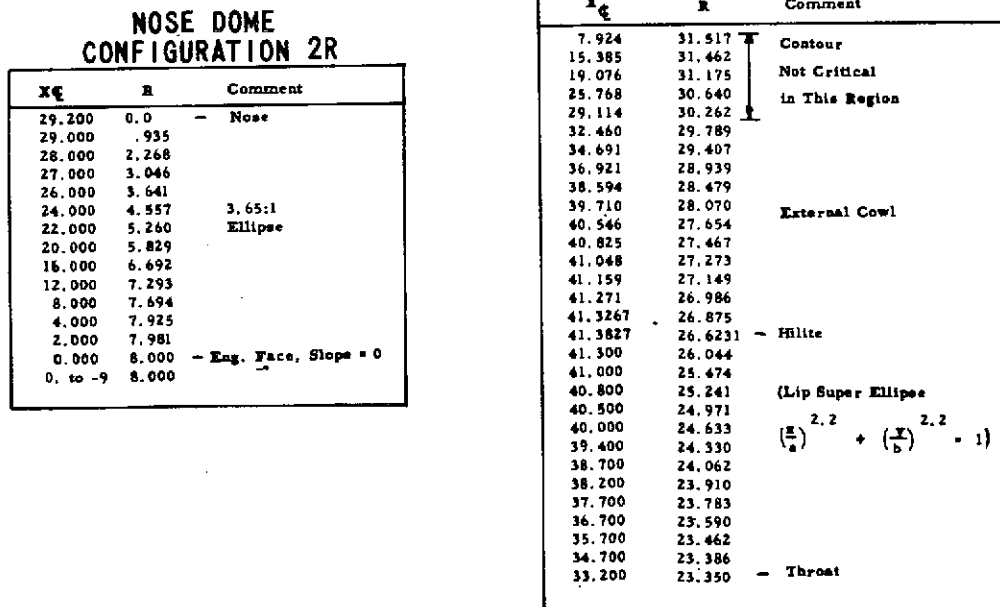
Modified NACA 0009 Airfoil

Preceding page blank

RING-CONFIGURATION 2R



LIP AND EXTERNAL COWL CONFIGURATION 1L



REFERENCES

1. Easterbrook, W. G., Roberts, W. H., The Boeing Commercial Airplane Company, "Low-Speed Wind Tunnel Flow Field Results for JT8D Engine on the Boeing 727-200", NASA CR Document, to be released.
2. Easterbrook, W. G., Carlson, R. B., The Boeing Commercial Airplane Company, "Cruise Drag Results from High Speed Wind Tunnel tests of NASA Refan JT8D Nacelles on The Boeing 727-200", NASA CR-134546, February 1974.
3. Bailey, R. W., Vadset, H. J., The Boeing Commercial Airplane Company, "727/JT8D Refan Side Nacelle Air Loads", NASA CR-134547, March 1974.
4. Pratt & Whitney Aircraft, "Phase I Engine Definition and Characteristics of the JT8D-100 Turbofan Engine", P&WA TM-4713, April 13, 1973.

THE FOLLOWING PAGES ARE DUPLICATES OF
ILLUSTRATIONS APPEARING ELSEWHERE IN THIS
REPORT. THEY HAVE BEEN REPRODUCED HERE BY
A DIFFERENT METHOD TO PROVIDE BETTER DETAIL